BNL-66820

CHAPTER XI

APPLICATION OF SYNCHROTRON RADIATION IN THE GEOLOGICAL AND ENVIRONMENTAL SCIENCES

Keith W. Jones

Brookhaven National Laboratory

Upton, New York 11973

To be Published in

Microscopic X-ray Fluorescence Analysis

Edited by

K. Janssens, A. Rindby, and F. Adams

John Wiley & Sons Ltd., Sussex, England

1999

DISCLAIMER

APPLICATION OF SYNCHROTRON RADIATION IN THE GEOLOGICAL AND ENVIRONMENTAL SCIENCES

Keith W. Jones
Brookhaven National Laboratory
Upton, NY 11973

1. Introduction

Scientists working in the geo- and environmental sciences are confronted with questions that cover size scales from the molecular to the cosmic. It is, therefore, not surprising, to realize that the analyses of relevant specimens are difficult and that the use of many different experimental approaches is required. The most obvious consideration is that these materials are highly heterogeneous so that analytical techniques must be capable of delivering information with a spatial resolution typical of grain sizes. Further, the physical geometry of rocks is important to measure to give the basis for improved theoretical calculations of fluid transport. Since many processes take place at highly elevated temperatures and pressures typical of petroleum reservoirs or the earth's core, it is appropriate to make these measurements under the same conditions. In many cases elements are present in trace quantities so that measurements must also be made with techniques that can detect minute amounts of elements throughout the entire periodic table. The chemical form of the compounds present in the material is required so that other types of approaches are needed to obtain this information.

In light of the difficult experimental challenges, scientists working on geological problems have been very ingenious, adventurous, and, in the end, successful in developing new analytical instrumentation and in applying many different types of existing methods in their experiments. Use of various types of light-, electron-, ion and x-ray probes has been

commonplace for many years. X-ray methods are particularly useful since x rays can be used for examination of large samples that are maintained at temperatures and pressures relevant to many situations found on the near-surface of the earth. Smaller samples can be examined at pressures found in the earth's core. Information on mineral structure, trace element concentrations, permeability, chemical speciation, and other parameters can all be obtained using x rays. When these factors are considered, it is plausible to assert that x rays provide the most useful single approach to analysis of geological specimens now in existence.

The applications of x-ray technology have been particularly stimulated by the development and application of x-ray beams based on the phenomenon of synchrotron radiation. While x rays produced in electron storage rings have been used for analyses of materials for approximately the past thirty years, the field is by no means mature. This is a result of rapid improvements in the performance of the storage rings and in the development of specialized insertion devices that locally perturb electron orbits to tailor the properties of the synchrotron radiation to specific requirements. The techniques for forming and detecting x-ray beams have made rapid progress and are still changing rapidly. As a result, the experimental methods for geological experiments have been enormously refined, thus enabling more sophisticated investigations. At the present time, a new third generation of synchrotron radiation sources is coming into full operation. For example, the European Synchrotron Radiation Facility (ESRF) at Grenoble, the Advanced Photon Source (APS) at Argonne National Laboratory, the Advanced Light Source at the Lawrence Berkeley National Laboratory, and the SPring-8 facility at Hyogo, Japan give x-ray beams with order-of-magnitude improvements in x-ray flux as well as extended energy ranges and reduced beam sizes. Older facilities such as the National Synchrotron Light Source (NSLS) at Brookhaven National Laboratory, the Cornell High Energy Synchrotron

Source (CHESS) at Cornell University, and the Photon Factory at Tskuba, Japan will be competitive and complementary to the third-generation facilities for many years.

The application of synchrotron radiation to the geological sciences has been reviewed by several authors in recent years (Bassett, 1988; Bassett and Brown, 1990; Smith and Rivers, 1995; Smith, 1995; Chevallier and Dhez, 1997; Török et al., 1998). The intent of the present review is to provide a survey of the field by concentrating mainly on presenting typical experiments that have been performed in the last five- to ten-year period. Details of the synchrotron source, beam line hardware, and background of experimental techniques can be found in the literature.

2. Synchrotron Radiation Experimental Beam Lines

The physical principles underlying the production of synchrotron radiation, details of electron storage ring design, parameters defining the operation of undulator and wiggler insertion devices, and beam line design lie beyond the scope of this discussion. The intent here is to present a bare minimum of information to illustrate the nature of the source and to give an idea of the appearance of a typical experimental arrangement.

The most important single parameter is the flux of photons that can be delivered to a sample. The flux from synchrotron sources is several orders of magnitude higher than the flux from rotating anode x-ray tubes. In turn, the flux from third-generation synchrotron sources compared to second-generation sources is also higher by three to four orders of magnitude. The higher flux is important in terms of reducing times for a given experiment, improving spatial resolution, and for reducing elemental detection limits. The energy distribution of flux produced at the APS is compared to that produced at the NSLS in Figure 1. It can be seen that at lower energies the NSLS is useful when compared to bending magnets at the APS, while the APS

undulators are clearly better for the ultimate in flux and also in providing a wider range of x-ray energies either with undulator or wiggler insertion devices. It should be noted that the flux values shown in Figure 1 do not include the use of focusing devices such as mirrors or capillaries (Chevallier and Dhez, 1997; Török et al., 1998). Their inclusion leads to further enhancements in flux of several orders of magnitude. Comparison of the ALS and the NSLS also shows complementary aspects in that the APS is ideal for lower energy experiments while the NSLS is an effective source of higher energy photons. There are, of course, other parameters defining the parameters of synchrotron radiation that come into play in the detailed design of particular experiments.

Formation of x-ray microbeams is of importance for several types of experiments. These methods have been discussed by Ice (1997); and in particular, the use of capillary focusing has been discussed by Bilderback et al. (1994), Pahl and Bilderback (1996), and Thiel et al. (1992). The capillary approach is attractive since it is inexpensive, is effective in producing beam sizes of 1 μm or less, and can enhance the photon flux by a factor of 100 or more.

X26A is a general-purpose microbeam facility at the NSLS that has been much used for x-ray fluorescence geological experiments. It can be used with several different types of beams:

- Collimated white beam. The routine beam size is about 8 micrometers but values to 1 μm have been employed. This has been widely used for synchrotron-radiation-induced x-ray emission (SRIXE) experiments.
- Focused white beam. This has not been used very much. Can be combined with the pinhole. Trace element detection limits are not much improved because of deficiencies in the mirror surfaces.

- Mono-energetic beam. Channel-cut silicon monochromator can cover the energy range between 4 and 17 keV. Routine use for x-ray absorption near-edge structure (XANES) and extended x-ray absorption fine structure (EXAFS) measurements with beams of about 200 micrometers for concentrations at the ppm level.
- Mono-energetic beam. Channel-cut silicon monochromator and Kirkpatrick-Baez mirrors. Beam size is less than 20 micrometers. Improved EXAFS and XANES performance.
- Capillary focusing to give beam size close to 2-5 μm. Intensity will be sufficient for SRIXE, EXAFS, and XANES work on trace elements at the ppm concentration range.

Trace element detection limits are around 10 fg for elements around Fe, Cu, and Zn using K-x ray detection and similar values for elements around lead using L-x ray detection. The useful energy ranges are up to about 50 keV for white beam and 17 keV for mono-energetic beams. A description of the beam line is given by Smith (1995).

The direct descendant of the X26A beam line is that produced by the University of Chicago Center for Advanced Radiation Sources (CARS) at the APS. A photograph of the experimental arrangement, as the experimentalist would see it, is shown in Figure 2 to give a feeling for the instrumentation to those not familiar with synchrotrons. Beam line details are to be found elsewhere and are not considered here since they are transparent to the user community. The photograph is taken looking down stream in the direction of the x-ray beam. The actual sample position is at the position of the 35-mm slide mount. The x rays are detected with a semiconductor x-ray detector that is seen on the left of the sample. The rectangular box on the right is an ion chamber used to monitor the x-ray beam intensity. The small objects between the ion chamber and the sample position are mirrors used to focus the x-ray beam in two dimensions.

It can be seen that the apparatus is basically simple and that it can be used effectively by a user community not necessarily expert in all the relevant synchrotron technologies.

3. Synchrotron Radiation Induced X-ray Emission (SRIXE)

Production of characteristic x rays by production of inner-shell vacancies by photo-ionization with x rays from a x-ray tube is a much-used analytical technique that can be applied across the entire periodic table. Synchrotron x-ray beams can replace those from a conventional tube and lead to instrumentation that delivers improved elemental detection limits and spatial resolution. The important factors for the synchrotron source are the production of high flux beams and almost complete polarization so that Compton scattering is almost completely eliminated as a source of background. Many approaches have been used for SRIXE instrumentation. Discussions of the techniques involved have been given by Jones (1992). The use of the x-ray microprobe should be considered as complementing other analysis devices such as the electron microscope. It will have a particular niche for analysis of the spatial distribution of trace elements. A number of illustrative applications are summarized below.

3.1. Extraterrestrial Materials

The study of extraterrestrial materials is an excellent example of the uses of SRIXE. There is generally a limited amount of material available so that the use of conventional chemical techniques is not possible either from considerations of the mass of material required for the application of conventional analytical techniques or from a desire for non-destructive methods that do not destroy the small amount of unique material that is available. SRIXE and XANES

meet these requirements since they give high detection sensitivity for elemental analysis, excellent spatial resolution, and chemical state analysis.

Delaney et al. (1996, 1998a, 1998b) have made an extensive study of the Fe^{3+}/SFe ratio in both terrestrial and extra-terrestrial specimens. They point out that the use of what they call synchrotron micro-XANES (SmX) can be used to do high spatial resolution measurements (10 μm × 20 μm) that show the results of zoning and oxide inclusions. The approach is based on determination of the energy of the pre-edge peak in the XANES spectrum and was calibrated by measurements of olivine, clinopyroxene, and tourmaline samples with known Fe^{3+}/SFe ratios of 0, 0.33, and 1 which were determined by wet chemistry. It was then possible to compare the results with those obtained by ordinary bulk chemical techniques with other samples of olivine, clinopyroxene, amphibole, biotite, and tourmaline. The results of the comparison between the SmX and bulk determinations using wet chemistry and Mössbauer measurements are shown in Figure 3.

This approach was used to determine the Fe^{3+}/SFe ratio in olivine, pyroxene, and feldspar found in thin sections of seven different Martian meteorites. Rather large variations are found in the measured ratios determined. Delaney et al. (1998a) present a discussion of possible mechanisms involved in the oxidation of the these meteorites, but, while on the one hand it is too early to draw firm conclusions, on the other hand, it is possible to say that the technical approach has demonstrated that the SmX method will be a very important tool for this type of study.

3.2. Fluid inclusions

Fluid inclusions represent a valuable source of data that describes the composition of fluids present during the process of the formation of ores from magmas and of minerals in general. The small volume of the inclusions and the interest in the composition of contained fluids or gases pose a challenging analytical problem. A number of analytical approaches have been used.

The direct extraction of the contained material followed by analysis using relatively conventional techniques such as laser ablation inductively coupled plasma mass spectrometry (LA-ICP-MS) is one very successful approach. An example is given by Audétat et al. (1998) who investigated the mechanisms of ore precipitation by study of the concentrations of some 17 elements in the liquid. Another method has been described by Ayora et al. (1994) who used x-ray analysis to make the elemental concentration measurements of the brine contained in the inclusions. The results were applied to the modeling of evaporite basins. The inclusions studied were found in halite from a location in the Messinian basin in Spain. The halite were placed on a cooling stage in a scanning electron microscope to freeze the fluids in the inclusions. The crystal was then cleaved to expose the frozen liquids to the electron beam. Conventional energy-dispersive detectors were used for the x-ray detection.

SRIXE represents an alternative method for determining the concentrations of materials found in the inclusions. The absorption lengths for the exciting x rays and for the exiting characteristic x rays are relatively large. Therefore, polished sections of rocks containing fluid inclusions can be analyzed without rupturing the inclusions, although great care is needed in the sample preparation so that the wall thickness of the inclusion is minimized. Mavrogenes et al.

(1995) have carried out an investigation of the difficulties of obtaining reliable data from fluid inclusions by using specially prepared artificial inclusions.

A totally different approach to this problem is to consider the use of synchrotron computed microtomography (CMT). Applications of CMT in the geosciences is discussed below in detail. Here, it should be mentioned that use of undulator sources at third-generation synchrotron x-ray sources will make it feasible to conduct detailed measurements of the volume of the inclusions as well as the distribution of trace elements in the fluids filling the inclusion based on detection of characteristic x rays. A simpler approach is to measure volumes above and below the absorption edge for the production of K-x rays from a specific element. Subtraction of the two volumes then gives the concentration distribution of that element (see Jones et al., 1991 for an example of the technique). Sample preparation will remain as a major problem in the application of the CMT technique since the size will be governed by the energies of the x rays from the elements of interest.

3.3. Ore Formation

Measurements of the composition of metal-bearing rocks is of interest from the standpoint of the mechanisms for ore formation and for providing data necessary for informed decisions about ore exploration and recovery procedures. An example is provided in the work of Chen et al. (1987) who investigated the occurrence of gold in unoxidized samples from the Carlin deposit in Nevada. The gold found in these deposits is very fine grained and is not readily visible using optical microscopy, but can be detected using the SRIXE technique. Two types of ore samples were examined. One was a limestone material and the other a breccia material. The samples prepared from these materials were 50 to130 μm thick and were mounted on mylar foils

200 μm thick. The SRIXE measurements were made on with x-rays from a NSLS bending magnet source. The beam size was 20 μm × 20 μm. The MDL for Au detection for a 900-s data accumulation time was 3 ppm. The results of the experiment showed that there was essentially no evidence that supported arguments for finding the gold in pyrite grains embedded in the ore. However, measurements carried out on non-carbonaceous material surrounding the pyrite grains showed the presence of gold in 9 of 17 locations. The x-ray spectra obtained for the pyrite and matrix locations are shown in Figures 4a and 4b, respectively. Extension of this type of experiment should help to illuminate the mechanisms involved in the formation of the ore deposits and by giving a more detailed understanding of the location of the gold in the ore could lead to improved recovery technology that is tailored to the chemistry of the specific material containing the gold.

An investigation of the occurrence of gold in micas has been conducted by Basto et al. (1995). The micas were from three sites in Portugal and included lepidolites from a lithium mine and muscovites from tungsten and gold mines as well as from a location which had no known mineralization. A synchrotron x-ray beam with an energy of 13 keV and size which was adjusted between 50 and 10^6 μm^2 and an acquisition time of 1000 s was used in the experiment. Quantitation of the results was found to be a problem since it was felt that there were no adequate reference standards available. For this reason, the results were normalized to manganese found in the samples as a minor element. The sensitivity of the measurement was sufficient to give reliable relative values for the gold concentrations even though a careful analysis of the spectra was required to account for possible interferences from other elements. It was also shown that there was linear correlation of Ga and Au with the sum of W and Ta concentrations, but there was no correlation for the pair of Au and Tl. The measured correlations are shown in Figure 5.

The elemental relationships are suggested as a possible useful indicator of the presence of trace amounts of gold that would be useful in prospecting for gold.

Secondary ion mass spectrometry is another analytical technolgy that can be used for measurement of trace elements in geological samples. Pratt et al. (1998) have used recent secondary ion mass spectrometry (SIMS) technology developments to make quantitative analyses of gold in pyrite. They analyzed secondary ions emanating from a 60-μm diameter area and observed the invisible Au concentrations as a function of depth into the sample for a surface layer of 0 to about 7 μm. The measurements show both the presence of invisible gold with constant concentration profiles and the presence of Au in well defined inclusions within the pyrite structure. The gold concentrations were around 10 ppm. The data extraction techniques give some insights into the chemical environment of the Au, that is, whether it is incorporated into the mineral structure or is present in colloidal form.

The experiments by Chen et al. (1987), Kucha (1993), and Basto et al. (1995) show that SRIXE and particle-induced x-ray emission (PIXE) can be used to provide sophisticated information on the occurrence of gold in different types of geological deposits and thus play a role in giving insights into the mechanisms in the ore formation. Application of higher intensity beams from third-generation synchrotron sources should extend the application by making possible XANES and EXAFS experiments on these low-concentration samples thereby adding information on the position of the gold in the matrix. A comparison of the XANES/EXAFS experiments with the environmental information inferred from the SIMS work would also be useful. In the future, it will be interesting to see if effective collaborations can be organized between the research groups and the actual mine operators so that the research results can be effectively applied to optimize industrial practices.

Dolbyna et al. (1995) have investigated ore forming processes in the ocean by analysis of microlayers of Fe-Mn nodules. These nodules were found in the abyssal deep of the Pacific Ocean at 9-18^0 N and 137-146^0 W at a depth of 4600 to 5200 m. The nodules rest on a surface composed of foraminiferal, radiolarial muds, and red clays and grow through diagenetic and hydrogenous processes. Maps were made of the distribution of elements in sections of the nodules with 20 keV x rays using a beam size of 250 μm and a step size of 500 μm for 2-dimensional maps and a beam size of 100 μm and step size of 250 μm for one-dimensional line scans. The 2-dimensional map produced an array of 56 × 56 pixels corresponding to an area of 28 mm × 28 mm. The distributions of Mn, Fe, Ni, Cu, Sr, Y, and Zr were determined along with a transmission x-ray image. The results suggest the existence of a surface region with a thickness of 3 to 6 mm on the equator and 2 to 3 mm on top and bottom followed by an intermediate ring and a central core. Enrichments in Mn, Ni, and Cu are found in the surface and intermediate layers and Fe, Sr, and Zr in the core. A line scan was measured along a line containing the surface and intermediate layers only. The results for the scan showing the enhancement at the surface regions are given in Figure 6. From the data presented, it is argued that the surface layers show the accretion of materials in modern times and that the changed conditions in the interior of the nodule reflects different environmental conditions in the past. The combination of the elemental microanalysis with age determinations of the layers will then make it possible to estimate the geochemical conditions as a function of geological times.

3.4. Determination of Metals in Sediments and Pore Water

The contamination of soils, sediments, and ground or pore water with toxic organic and inorganic compounds is a matter of great importance for the environment. Improved

understanding of the distribution of these compounds at the grain- or pore-scale level is needed in order to serve as the foundation for refined transport calculations and for devising appropriate decontamination treatment strategies. These topics have been considered by Olsen et al. (1982). They list a number of different mechanisms that are important in binding contaminants to sediment particles and present examples of transport in several different locations. The importance of obtaining data on surface morphology and surface chemical characteristics as the basis for understanding transfer mechanisms between phases is obvious. As pointed out by Olsen et al. (1982) microanalysis techniques "..have an advantage in that one can observe directly the nature of the particulate matter, associations of different particle types, chemical inhomogeneities along the surface that may result in large differences in chemical reactivity, and specific particle-pollutant associations." Even though Olsen et al. published their review in 1982, these observations remain valid today. Progress in microbeam techniques since that time has been substantial so that it is now possible to consider particle-scale (micrometer-scale) experiments that will help to give detailed answers to these points. Metals in sediments can be adsorbed on the particles either as a consequence of scavenging by Mn-, Fe-oxides or displacement in silicates, or as a consequence of formation of chelate-type complexes due to the presence of organic matter on the particle surface. The particle-reactive metal contaminants can then be transformed by adsorption-desorption in sediments due to redox reaction, organic matter biodegradation, ion exchange, etc. Besides grain sizes which determine the specific surface area of the particles, the composition and structure of the particles and organic matter content associated with the particles are other important factors determining the concentrations of contaminants. The cation exchange capacity (CEC) (Drever, 1988) of clay minerals determined by their micro-scale structures and compositions, can significantly affect the adsorption-

desorption of contaminants, and, therefore, the transfer of contaminants from one medium to another (e.g., sediment-water) and the partitioning between solid phase and pore water. The migration and transfer of contaminants in sediments through pore space is an important mechanism determining contaminant distribution. The sediment structure, porosity, permeability, tortuosity, chemical properties, and so on are factors that determine the diffusion, migration, and transport of contaminants in sediments and the diffusive flux of contaminants inside the sediments and between sediments and overlying water through pore space. Through micro-analysis of sediments, it may be possible to obtain experimental information to define the parameters of contamination diffusion and transport, rather than estimating the value of those parameters as is done in a traditional way. The accurate measurement of the sediment structure and pathways of contaminant transport through micro-scale analysis should also provide new key information on geochemistry, geology, clay mineralogy, and contaminants for the sediments studied.

An interesting method for analysis of pore waters and individual grains of particles has been described by Grime and Davison (1993). Their work was based on the use of PIXE which is the analog of SRIXE and Rutherford backscattering (RBS) for which there is no direct analog. The experiment is described here in the hope that it will stimulate work to modify the approach for use with SRIXE. They relied on diffusive equilibrium between the pore water and a thin film of polyacrylamide gel inserted into the sediment surface. Equilibrium between the pore water and the gel is achieved in a matter of hours. Following exposure, the gel is treated to prevent any diffusion of metal ions. In the case of iron, this was done by exposing the gel to 1 mmol/l NaOH solution in order to convert the element of interest, iron, to iron oxide precipitation, e.g., ($Fe_2O_3 \cdot 3H_2O$). The gel was mounted in a holder which exposed only one surface to the sediment.

Analysis of the clean side was then possible by choosing a thickness of gel sufficient to absorb x-rays from the side exposed directly to the sediment.

Measurements were made with a proton beam current of 100 pA and a beam size of 100 μm^2. The detection limit for iron was found as low as 0.2 mg/ℓ in the pore water. The results of the analysis are shown in Figure 7. The slope of the dissolved Fe curve with depth near sediment-water interface can be interpreted in terms of a model for iron supply to the sediments to give estimates for the diffusive flux of iron to the sediments from the overlying water.

It is also possible to measure the stoichiometry of individual particles less than 1 μm size (or greater than 0.4 rem) obtained by filtering the water in an anoxic lake. The particulate Fe and S concentrations on the filter were mapped and showed regions where the Fe concentration was enhanced relative to the S concentration. The geochemistry of Fe and S in an anoxic environment is beyond the scope of this discussion. However, the fact is this technique provides geochemists with a powerful tool to study the formation of clay minerals. RBS spectra allowed the determination of the Fe/S and Fe/O ratios which were found to be consistent with those expected for iron sulfide, ferrihydrite, magnetite, or haematite. The results show that the iron oxides can exist in an environment dominated by the sulfides. This technology has a great potential to bring a new era of geological, geochemical, and clay mineralogical studies in earth science.

The management of dredged material in the Port of New York/New Jersey is another particular example of the need for the type of information mentioned above. The Port requires dredging on a regular basis to maintain the port channels at an adequate depth. Recent environmental actions have made it difficult to use the traditional ocean dumping method for disposal, and it is now necessary to find other solutions. Contaminant transport models can help

in programs designed to reduce the volume of material that must be dredged and to reduce the input of contaminants into the system. Studies at the grain size and mineral structures are an essential component of understanding the geochemistry involved in binding contaminants to the sediments and in devising effective removal methods based on an understanding of the speciation, partitioning, and transport mechanisms. Many aspects of the overall problem have been summarized recently (U. S. Environmental Protection Agency, 1998; National Research Council, 1997).

Synchrotron radiation methods can be applied very effectively to sediment studies. Transitional elements (e.g., heavy metals) can be particularly well characterized using SRIXE since this technique provides the combination of spatial resolution and excellent detection sensitivity required. The use of XANES and EXAFS provides chemical structural information not given by other techniques. Infrared microscopy can be used for measuring surface chemical compositions. Microdiffraction methods can be used to determine the composition of individual grains. These approaches can be coupled with use of electron and ion beams and other analytical approaches.

Song and Jones (1997) have used SRIXE to investigate individual particles from a location typical of contaminated sediments found in the Port of New York/New Jersey. This location was in Newtown Creek which is a small waterway running east from the East River between the Boroughs of Brooklyn and Queens on Long Island. This initial work looked at relatively large particles (> 63 μm) and did not attempt to work with the very fine grained silts and clays (< 63 μm) which form the major fraction of the sediments. Measurements were made with a white beam from a bending magnet at the NSLS at Brookhaven National Laboratory collimated to sizes of about 15 μm. Specimens of the as-dredged sediment were placed on a 7-

μm polyimide backing. Fine-grained inorganic particles, which have presumably a certain amount of organic materials on the surface, and organic particles, if any, in a few-micrometer size could have also be included as silts and clays fractions. Measurements were made of the contaminant concentrations on a number of particles in several grain-size groups. Results found for the distribution of lead are shown in Figure 8. It can be seen that there is a general level of contamination on all particles. This implies that the contamination has been spread by a diffusive as well as advective mechanism rather than just being the result of the physical transport of smaller numbers of highly contaminated particles from a few point sources. Line scans were also made across several of the particles in an effort to see if a determination of the relative importance of surface and volume contaminant levels. In principle, it should be possible to estimate the surface concentrations by the presence of an enhanced yield at the edge of the particle compared to the yield at its center. The results of one such scan are displayed in Figure 9. There is some evidence for a surface peaking. This could be caused either by preferential adsorption and/or ion exchange of metal contaminants at the edge (surface) of particles which are usually negatively-charged due to loss of cations, or that the spatial resolution used in the scan was large compared to any surface layer and thereby reduces the magnitude of the effect. The results do indicate that further work using higher resolution will help to yield definitive information on the contaminant distributions.

3.5. Detection of Rare Earth Elements

The detection of rare earth elements, and more generally elements with A~100, can be difficult using conventional x-ray fluorescence or electron probes because of the overlaps between the K- x rays from lighter elements and the L-x rays from the heavier elements. SRIXE

can be applied advantageously to solve these problems. Wavelength dispersive detectors used in conjunction with undulator sources give improved separation of the closely spaced x rays by reason of their improved energy resolution. Alternatively, the high energy x rays from synchrotron sources such as the APS can be used to produce heavy element K x rays which are suitable for analysis using energy dispersive x-ray detectors.

An example of the latter approach is given by an experiment performed by Chen et al. (1993). They used a 6-T wiggler beam line at the NSLS collimated to 25 μm for the work. Samples of rare-earth element rich ore from the Bayan Obo deposit in China and synthetic high-silica glass were examined. The spectra obtained for the two samples are shown in Figure 10. Analysis of the data gave values for the minimum detection limits of 6 ppm for La rising to 26 ppm for Lu. The experiment shows that the SRIXE method gives improved detection limits when compared to electron probe analysis, detection limits comparable to instrumental neutron activation analysis, and detection limits with excellent spatial resolution suitable for analysis of individual mineral phases. The experiment shows the applicability of the technique for study of the ore petrogenesis and for understanding granitic evolution by examining partitioning of rare earth elements between melt and vapor phases.

3.6. Trace Elements in Minerals

Trace elements found in minerals in general can be used to gain an understanding of the conditions under which they were formed. An example is given in a study of cleat-filling calcite in Illinois basin coals carried out by Kolker and Chou (1994). They studied the microdistribution of Mn, Sr, and Fe in 15 samples from several active mines. The SRIXE experiment was performed at the NSLS using an x-ray beam size of about 10 μm. Two-dimensional maps of the

Fe, Mn, and Sr distributions in one sample are shown in Figure 11. The concentrations are highest for the light areas of the maps and lowest for the dark areas. The measured concentrations vary widely: Fe from 52 to 16,700 ppm, Mn from 786 to 9480 ppm, and Sr from <5 to 461 ppm. This variation can be seen in the maps and show the zoning in the calcite formation. Kolker and Chou use the results of the synchrotron experiment in conjunction with data from other workers to argue that the cleat-filling calcites were precipitated from fluids similar to present day waters having a meteoric source.

This type of experiment should have wide application in studies not only of coal, but other types of minerals. The low detection limits, ease of quantitation, and high spatial resolutions typically found in SRIXE (and PIXE) experiments represent a major improvement over the results that can be obtained by use of other methods and make likely the extension of this approach to a wide variety of minerals.

4. X-ray Diffraction

X-ray diffraction (XRD) analysis of materials is a method for determination of the structure of materials that has been intensively used for most of the 20th century. Nonetheless, it still remains as the basis of many of the most vital areas of scientific investigations. The use of synchrotron radiation has expanded the types of experiments that can be done by making possible the investigation of small-size samples.

This is illustrated in an experiment performed at the ESRF by Pluth et al. (1997). They provide an interesting overview of the need for additional structure determinations, the reasons why the developments in synchrotron radiation sources are important for the field, and list some of the difficulties associated with measurements of small crystals. In particular, it would seem

that the mention of problems associated with extracting proper crystallographic for the sample because of changes in structures at surfaces also points out the use of the high-spatial resolution XRD specifically for measurements of surface structures.

The mineral chosen for examination was Raite, which is a mineral found on the Kola Peninsula in Russia. They used a 30-μm beam to investigate a Raite crystal that had dimensions 3 μm × 3 μm × 65 μm giving an exposed volume of about 300 μm^3. It was pointed out that the x-ray beam intensity was sufficient for work with even smaller volumes. The x-ray data was accumulated using a charge-coupled device (CCD) area detector to obtain 73 frames as a function of angle. Analysis of the data was done using standard programs and gave lattice constants and positional parameters for the Raite crystal. Interestingly, the valence state of Mn in the crystal was found to be uncertain and it was suggested that this discrepancy could be resolved using synchrotron XANES and EXAFS measurements.

An exploratory measurement on a specimen of silicate perovskite which had been laser-melted in a small 10-μm diameter spot was made by Jones et al. (1996). A 2-μm beam was obtained using a capillary for focusing. In this experiment, diffraction patterns were observed using both CCD and image plate detectors. The image obtained at with the image plate detector at one location is shown in Figure 12, and the image obtained with the CCD device when the beam irradiated the rock at another location is shown in Figure 13. Clear differences can be seen in the diffraction patterns. In addition, data collection times when using the CCD detector are of the order of 1 s so that it was possible to map the entire region using a spatial resolution of 2 μm and taking points at the same intervals. The pictures obtained were recorded on video tape for later analysis. The ability to study changes in crystal structure with this type of spatial resolution

will be generally useful, although the analysis of the large amounts of data accumulated is a challenging problem.

5. High-pressure Experiments

Investigation of the properties of geological materials at elevated pressures and temperatures is a particularly fascinating topic since experiments that relate to the extreme conditions found in the earth's interior and in planetary material can be carried out under similar conditions. The state-of-the-field has been examined thoroughly in a series of recent reviews. Consideration is given to recent developments in instrumentation, *in-situ* properties of materials, partitioning/segregation, and iron in the earth's core. X-ray techniques are one of the most important methods used for characterizing these materials. Since the sample sizes are small the use of x-ray beams from synchrotron x-ray sources has become extremely important in the field. The instrumentation used in the synchrotron experiments is described by Brister (1997) and the design of a dedicated facility for high-pressure research at the APS has been covered by Rivers et al. (1998).

Investigations of iron at the pressures and temperatures of the earth's interior have been investigated intensively because it is the major component of the core and must, therefore, be a dominant factor in determining its functions. High-pressure experiments have been crucial in determining the phase diagram as a function of temperature and pressure. Anderson (1997) has reviewed the present status of the investigations and specifically points out how the improved x-ray intensities from the synchrotron x-ray source have been essential for the experimental work. A summary phase diagram of iron is shown in Figure 14. Major points of uncertainty remain as well as the need to extend the work to higher temperature and pressure regimes. Andrault et al.

(1997) performed an experiment at the ESRF which exemplifies many aspects of the high-pressure experiments and resolves some of the questions surrounding the phase diagram. The experiment used a diamond anvil cell to cover a pressure range from 30 to 100 GPa and laser heating to achieve temperatures up to 2375 K°. Mono-energetic x-rays with an energy of 0.4245 Å were produced by an undulator and channel-cut silicon monochromator and then focused with mirrors to a final size of 15 μm by 8 μm. Angle-resolved measurements with image plate detectors were feasible for the first time using this equipment. The variation of the diffraction spectra obtained as a function of temperature at a pressure of 44.6 GPa is shown in Figure 15. The measurements showed the existence of a phase transformation for iron in the temperature-pressure region investigated.

Another study related to a phase transformation of importance to structure of the earth's mantle was performed at the SPring-8 facility by Irifune et al. (1998). They examined the phase boundary between olivine and spinel structures with white x rays from a bending magnet beam line. The beam was collimated by horizontal slits to 100 μm and by vertical slits to 200 μm. A 100-μm horizontal slit collimated the diffracted x rays. The diffracted x rays were observed with a Ge x-ray detector place at $2\theta = 5.0°$. These conditions are to be contrasted with the undulator experiment performed by Andrault et al. (1997) just discussed. Energy-dispersive diffraction spectra are shown in Figure 16 for several temperatures and pressures. Analysis of the spectra gave the phase boundary as a function of pressure from 1400 to 1800 C° and will improve understanding of the nature of seismic discontinuities in the earth's mantle at 410- and 660-km depths.

6. Computed Tomography Experiments

Computed microtomography (CMT) using x-ray beams from a synchrotron is a natural extension of a technique that has been widely applied in science, industry and medicine for many years. Images can be produced based on measurement of x-ray absorption coefficients, detection of characteristic x-rays or diffracted x-rays from specific elements or crystals. Herman (1980) has described the fundamental methodology. Kinney et al. (1992) have surveyed the field of synchrotron CMT and D'Amico et al. (1992) describe the CMT beam line developed by EXXON at the NSLS. A survey of industrial applications of various types of tomography has also been made that gives a good overview of some of the underlying principles of tomography (Scott and Williams, 1995).

There are several general types of applications of the technique. The structure of different types of materials is one example. Verhelst et al. (1996) and Simons et al. (1998) have studied the coal components vitrinite, liptinite, inertinite, pyrite and voids and compared the results with optical visualizations. Carlson and Denison (1992) studied the size and spatial distribution of garnet crystals in a study of the mechanisms of porphyroblast crystallization. Void and fracture structures are another general topic. An example is given by Johns et al. (1993) who carried out nondestructive measurements of fracture apertures in crystalline rock. Finally, the structure of porous media and fluid flow in these media is of great importance for petroleum recovery and for understanding the fate and transport of different types of environmental contaminants. Examples of this type of application are described by Wang et al. (1985) and Kantzas (1990). The general field of tomography applied to soils has been summarized (Anderson and Hopmans, 1994) and the possible uses of synchrotron radiation in the field by Spanne et al. (1994a).

The most widely applied tomographic imaging technique is based on measurement of the linear x-ray absorption coefficient as an x-ray beam passes through a specimen. A typical experimental arrangement is exemplified by an instrument recently put into operation at the BNL NSLS (Dowd et al.,1998). An area x-ray detector is employed so that the tomography experiment requires only the measurement of the transmitted x rays as a function of angle. A schematic diagram of the apparatus is shown in Figure 17. The x-ray detector is a YAG:Ce scintillator viewed through a magnifying lens by a charge coupled device area photon detector. The system resolution is approximately 2.7 μm. The resolution and, hence, the size of the image, can be adjusted by varying the magnification of the viewing lens. The mathematical techniques used to produce the tomographic image is a topic that stands alone. Discussions of several approaches are given in the literature cited here.

An alternate method, a first-generation CMT apparatus, uses a pencil beam formed by a collimator to measure the attenuation of a single ray that traverses the specimen. The needed data is accumulated by stepping the beam across the sample and at each point accumulating a set of measurements as the specimen is rotated through 180°. The effective pixel size is determined by the step size taken in the lateral scan of the specimen. The data obtained can then be used to reconstruct a single tomographic slice. A volume display can then be obtained by sequential measurements at different positions along the axis orthogonal to the plane of the sections. While the first-generation method has been generally abandoned in favor of the third-generation (area detector) method, it may still have specific utility for making very high resolution measurements based on collimating the x-ray beams by sub-micrometer diameter capillary optics or for tomography based on detection of characteristic x rays emitted by the sample material.

The general topic of flow in porous media is important in several fields including petroleum recovery and transport of contaminants in soils, sediments, and rocks. CMT can be applied in measurements of the microstructure of these materials, the movement of fluids through the microstructures, and in looking for changes in surface composition caused by fluid-solid interactions. Investigations focused on aspects pertinent to the petroleum industry serve as an excellent specific example.

Experimental measurements on sandstones are of basic interest for understanding fluid flow in petroleum reservoirs. The sandstone structures were studied using a first-generation CMT apparatus by Spanne et al. (1994b), by Coles et al. (1996,1998a, 1998b) who used first-generation equipment and a beam from a 6 T superconducting wiggler at the NSLS as well as the third- generation equipment described by Dowd et al. (1998), and Auzerais et al. (1996) who used third-generation apparatus at a NSLS bending magnet beam line.

Spanne et al. (1994b) studied a sample of Fontainebleau sandstone with the objective of characterizing the microgeometry of the rock. The experiment employed a 5 μm × 5 μm white beam from a NSLS bending magnet. A 100-μm Mo filter eliminated low energy photons to give a mean beam energy of 19 keV. The data was accumulated in the form of 100 slices with a size of 303 × 303 pixels. The pixel size was 10 μm × 10 μm and the spacing between sections was also 10 μm. The analysis of the data gave values for the porosity, formation factor, the ratio of the macroscopic conductivity of the rock, and the conductivity when filled with a conducting liquid phase, and the permeability. Good agreement was obtained between these calculated values and results obtained using other methods.

Coles et al. (1996, 1998a, 1998b) studied a high permeability reservoir sandstone using the first-generation BNL CMT scanner and x-rays produced with a 6.4-T superconducting beam

line. A 6 mm sub-volume of a 2.54 cm diameter x 3.18 cm sandstone plug was imaged at a resolution of 30 μm. Measurements were made on the sample when it was dry, and on the residual oil left after first filling the rock with oil and then displacing the oil with brine. The results obtained for individual slices through the sandstone along the three-different axes and for the entire tomographic volume are shown in Figure 18. The three-dimensional distribution of the water alone is shown in Figure 19. Validation of the predictions of fluid dynamics models can be made with the pore-scale experimental data obtained from the CMT work. Results of such a comparison of the CMT experimental results shown in Figures 18 and 19 with calculations performed at Los Alamos National Laboratory using a lattice Boltzmann model are displayed in figure 20 where the experimental data for four slices are compared to the model calculations. In addition, calculations can be made using a network and percolation models to simulate the changes between equilibrium states (Hazlett, 1995) are also shown. This general approach has been extended by Coles et al. They used the third generation apparatus described by Dowd et al (1998) to investigate a North Sea Brent sandstone with a permeability of .470 Darcy. The results obtained for individual slices and for the tomographic volume are shown in Figure 21. This data can be analyzed to show spatial correlations, connectivity, and tortuosity (Lindquist et al. (1996)) and compared to the fluid dynamics and network modeling calculations already mentioned. The excellent spatial resolution makes it feasible to consider investigations of the fluid-rock interactions on a pore-scale by determination of surface composition and wettability that have not been feasible in the past.

Auzerais et al. (1996) and Schwartz et al. (1996) independently carried out a similar program for investigation of transport in sandstone during the same time period covered by the work described above. They performed high-resolution CMT measurements of Fontainebleau

sandstone at the NSLS and calculated values for porosity, pore-volume-to-surface ratio, permeability, electrical resistivity, and several other parameters from the data. The values were compared with experimental results obtained for larger samples and generally good agreement was found. Poorer agreement was found for parameters such as the resistivity which involve more complex model calculations.

The two experiments taken together are convincing evidence for the power of CMT in fluid transport studies. They show how CMT can be used in conjunction with industrial CT scanners, magnetic resonance imaging, and other conventional analytical techniques for obtaining refined understanding of transport at the pore-scale dimension that can be used as the foundation for understanding fluid transport on larger size scales.

The high x-ray intensity produced by synchrotron sources can be used to bring tomography-based x-ray fluorescence into use as a practical analytical method. The type of sample that can be examined will be defined by the energy of the fluorescent x rays. Synchrotron fluorescent tomography was demonstrated more than ten years ago at the NSLS by Boisseau (1986). They used first-generation equipment and a Si(Li) x-ray detector to measure the distribution of Fe in a bumble bee. Hogan et al. (1991, 1993) investigated computer models that corrected for absorption of the fluorescent x-ray materials. More recently. Janssens et al. (1998) working at Hasylab in Germany measured fluorescent tomograms for S, Ca, V, Cr, Fe, Ni, Cu, Zn, and Mo in fly ash particles. The pixel sizes were about 4 μm. A section through a particle for these 9 elements is shown in Figure 22 Some, but not all, of the elements show evidence for higher concentrations at the edge of the particle. There are also some that show the presence of grains forming the overall composite ash particle. The ultimate success and usefulness of fluorescent tomography for trace or minor element mapping are heavily dependent

on the use of third-generation undulator sources so that the highest possible x-ray intensity is obtained.

Obtaining the best spatial resolution for CMT clearly continues to be a major technical goal. The present systems operate with voxel sizes of several micrometers at best. This value is to be compared to the voxel sizes of about 0.1 μm that have been obtained using MeV ion beams at the University of Oregon (Schofield and Lefevre, 1992) and the University of Melbourne (Cholewa et al., 1994). The contrast mechanism used for ion-beam tomography is based on a measurement of the energy loss of the particles in the sample. This is strongly dependent on the mean atomic number of the sample. Hence, it is possible to distinguish between variations in light element composition using ion beams than it is using x-ray beams. Ion beam technology is best suited for high-resolution measurements of objects of relatively small objects because of the rapid loss of energy in the sample. Efforts to obtain improved resolution for x-ray tomography in the same range is being actively pursued using a number of different methods, but none have been put into active practice for experiments as yet. For example, two efforts have been reported by groups working at the ESRF that are based on use of phase contrast occurring at the boundaries of features found in the sample when observations of the x rays are made at distances of a few centimeters from the sample (European Synchrotron Radiation Facility, 1997; Raven et al., 1997; Koch et al., to be published; Cedola et al., 1998).

7. XANES and EXAFS

EXAFS and XANES are techniques widely employed using x-ray beams from both laboratory sources and synchrotron sources. Measurements based on a direct measurement of the sample x-ray beam transmission for study of major and minor elements in a sample are fairly

straightforward. The use of several different types of x-ray detectors has made it feasible to extend the measurements to trace element concentration levels and with improved spatial resolutions. Of course, spatial resolution may not be of major importance for many studies where homogeneous samples are readily available. Applications of the techniques can be illustrated by focusing on investigation of sediment and fossil fuel applications.

Vairavamurthy et al. (1995, 1997) have carried out an investigation of the chemical forms of sulfur found in sedimentary humic substances. It is pointed out that humic materials maybe of importance in the formation of petroleum and that they also will interact with organic and inorganic contaminants in the water and are thereby important in controlling the fate and transport of the contaminants. Problems of contamination in New York Harbor and SRIXE experiments were described above from the standpoint of metals found in the sediments. Studies of humic substances in terms of contaminant fate and transport are very necessary to understand how the humates are distributed relative to the sediments and how the contaminants are bound to the humates and to the sediments.

Vairavamurthy et al. (1995, 1997) studied the behavior of sulfur found in sediments from a Shelter Island, New York salt marsh, Florida Bay, and the Peru margin using XANES and other analytical techniques. Results for the XANES spectra for the near-surface water-washed sediments and humic acid extracted from the sediments are shown in Figure 23. Interpretation of the spectra rests on accumulating a set of spectra from sulfur compounds that are contained in the sediments and the humic acids. A set of the calibration spectra that were obtained are shown in Figure 24. The compounds are classified in terms of their degree of oxidation and reduction states. The calibration spectra can be used to fit the sediment and humic acid XANES results and thus give a determination of the sulfur compounds found in them and their concentrations in

the sediment. The result of doing this fit for humic acid and sediment from the New York salt marsh is shown in Figure 25. The chemistry of sulfur in the sediments can be followed as a function of depth to give an extensive view of the chemistry of a very complex system. These experiments are focused on a single element, but the general approach is applicable to most or all elements so that the chemistry of other elements can be investigated in a similar fashion.

Coal is a geologic material that merits study for several reasons. From a basic standpoint it is a material which contains a record of past geological history that is especially useful because of the incorporation of organic materials not found in rock. From a practical standpoint it is a major fuel so that questions related to combustion are important as is gaining understanding of the impact on the environment and human health from the toxic organic and inorganic compounds emitted during the combustion process. The heterogeneous nature of coal makes high spatial resolution synchrotron x-ray techniques a useful and perhaps unique method for gaining improved understanding of coal formation and end use. However, measurements on bulk samples are also especially needed for dealing with combustion related problems. Work carried out over a number of years by a group from the University of Kentucky illustrates experiments utilizing bulk samples (G. P. Huffman et al., 1989; N. Shah et al., 1993; N. Shah et al., 1995).

Shah et al. (1993) measured both the concentration and form of As, Cr, Mn, and Ni using EXAFS/XANES spectra measured through detection of the K x rays. Results for the As spectra obtained for a number of different coal specimens are shown in Figure 26. Substantial differences are found for the form of the As contained in six samples analyzed. The As can easily oxidize from the arsenical to the arsenate form so that care in sample storage and handling

is necessary. It is pointed out that the combustion process will result in the conversion of all arsenic forms to the arsenate form.

Shah et al. (1995) also showed that *in-situ* x-ray absorption measurements could be performed on samples contained at pressures up to 123 atmospheres and temperatures up to 500 °C in a cell using thin layers of graphite cloth that were weakly absorbing enough to allow the passage of a 7-keV x-ray beam. This cell was used to investigate the behavior of Fe-based catalysts used for coal liquefaction. The results of the work give refined insights into how the catalysts function via direct measurements at the temperature and pressures used for coal liquefaction. This type of *in-situ* experiment is clearly generally applicable for examination of combustion-related processes.

8. Summary

A survey of some of the different ways that synchrotron x-ray beams can be used to study geological materials has been presented here. This field developed over a period of about 30 years, and it is clear that the geological community has made major use of the many synchrotron facilities operating around the world during this time period. This was a time of rapid change in the operational performance of the synchrotron facilities and this in itself has made it possible for geologists to develop new and more refined types of experiments that have yielded many important results. The advance in experimental techniques has proceeded in parallel with a revolution in computing techniques that has made it possible to cope with the great amount of data accumulated in the experiments.

It is reasonable, although risky, to speculate about what might be expected to develop in the field during the next five- to ten-year period. It does seem plausible that the rate of change

in the performance of what might now be called conventional x-ray storage rings will slow. There are no new facilities that are superior to the ESRF, ALS, APS, or SPring8 facilities under construction or about to come into operation. Thus, performance increments in the characteristics of the x-ray sources may come through the introduction of specialized devices in existing storage rings. The free electron laser is one example of a developing new technology that should take us into new regions of performance for radiation sources and stimulate new types of experimental applications.

It is also likely that major advances will come through the introduction of more sophisticated experimental devices developed for use with the very recently operational undulator or wiggler sources at the newer rings. Improved x-ray optics and x-ray detectors and more powerful computation and high-speed data transmission can bring about more refined experiments and make the synchrotron facilities more widely available to the experimental community. The next years should therefore be a time of high productivity and great excitement quite comparable to the previous era of synchrotron-based geological research.

9. Acknowledgments

I wish to thank Lore M. Barbier and Huan Feng for critical comments and crucial assistance in the preparation of this manuscript. My initial introduction to the material covered in this chapter came from Joseph V. Smith, Mark L. Rivers, and Steven R. Sutton of the University of Chicago. They have been a source of information and inspiration for many years. I am also indebted to many other collaborators some of whom are named or referred to in the material covered in this chapter, but will not attempt to enumerate them all. However, it is appropriate to make a special and heartfelt acknowledgment to the contributions of Per Spanne

who died in the September 1998 crash of Swiss Air Flight 111. Per was a very patient teacher and a wonderful colleague for many of us at BNL and at the ESRF. He was the originator of work in computed microtomography at Brookhaven for many years and was the leading spirit in many elegant experiments both at Brookhaven and later at the European Synchrotron Radiation Facility.

This research is supported in part by the US Department of Energy, Office of Basic Energy Sciences, Engineering and Geosciences Division, Contract No. DE-AC02-98CH10886.

9. References

Orson L. Anderson, Iron: Beta Phase Frays, Science 278:821-822 (1997)

Stephen H. Anderson and Jan Hopmans, editors, Tomography of Soil-Water Root Processes, Soil Science Society of America, SSSA Special Publication Number 36, Madison, Wisconsin, 136 pp. (1994)

G. Andrault, M. Fiquet, F. Kunz, F. Visocekas, and D. Haüsermann, The Orthorhombic Structure of Iron: An in Situ Study at High-Temperature and High-Pressure, Science 278:831-834 (1997)

A. Audetat, D. Gunther, and C. A. Heinrich, Formation of a Magmatic-Hydrothermal Ore Deposit: Insights with LA-ICP-MS Analysis of Fluid Inclusions, Science 279:2091 (1998)

F. M. Auzerais, J. Dunsmuir, B. B. Ferréol, N. Martys, J. Olson, T. S. Ramakrishnan, D. H. Rothman, and L. M. Schwartz, Transport in Sandstone: A Study Based on Three Dimensional Microtomography, Geophysical Research Letters, 23:705-708 (1996)

C. Ayora, J. Garcia-Veigas, J. Pueyo, X-ray Microanalysis of Fluid Inclusions and Its Application to the Geochemical Modeling of Evaporite Basins, Geochim. Cosmochim. Acta 58:43-55 (1994)

W. A. Bassett, Synchrotron Radiation, Applications in the Earth Sciences, EOS 69:1675 (1988)

W. A. Bassett and G. E. Brown, Jr., Synchrotron Radiation: Applications in the Earth Sciences, Annual Review of Earth & Planetary Sciences 18:387-447 (1990)

M. J. Basto, M. O. Figueiredo, F. Legrand, P. Chevallier, Z. Melo, and M. T. Ramos, Gold Assessment in Micas by XRF Using Synchrotron Radiation, Chemical Geology 124:83-90 (1995)

Donald. H. Bilderback, Stephen A. Hoffman, and Daniel J. Thiel. Nanometer Spatial Resolution Achieved in Hard X-ray Imaging and Laue Diffraction Experiments. Science 263:201-203 (1994)

P. Boisseau, Determination of Three Dimensional Trace Element Distributions by the Use of Monochromatic X-Ray Microbeams, Ph.D. Thesis, Massachusetts Institute of Technology (1986)

K. Brister, X-ray Diffraction and Absorption at Extreme Pressures, Rev. Sci. Instrum., 68:1629-1647 (1997)

W. D. Carlson and C. Denison, Mechanisms of Porphyroblast Crystallization: Results from High-Resolution Computed X-ray Tomography, Science 257:1236-1239 (1992)

J. R. Chen, E. C. T. Chao, J. A. Minkin, J. M. Back, W. C. Bagby, M. L. Rivers, S. R. Sutton, B. M. Gordon, A. L. Hanson, and K. W. Jones. Determination of the Occurrence of Gold in an Unoxidized Carlin-type Ore Sample Using Synchrotron Radiation. Nucl. Instrum. And Methods in Phys. Res. B22:394-400 (1987)

J. R. Chen, E. C. T. Chao, J. M. Back, J. A. Minkin, M. L. Rivers, S. R. Sutton, G. L. Cygan, and J. N. Grossman, Rare Earth Element Concentrations in Geological and Synthetic Samples Using Synchrotron X-ray Fluorescence Analysis, Nucl. Instrum. Meth. in Phys. Res. B75:576-581 (1993)

P. Chevallier and P. Dhez, Hard X-ray Microbeam Production and Application, in Accelerator-based Atomic Physics Techniques and Applications, S. M Shafroth and J. C. Austin, editors, Chapter 10, 309-348, American Institute of Physics, New York (1997)

M. Cholewa, G. J. F. Legge, A. Saint, J. Howard, and D. Whitehouse, High Resolution 3-D Tomography Using Ion Beams. Annales de Chimie 19:245 (1994)

M. E. Coles, R. D. Hazlett, E. L. Muegge, K. W. Jones, B. Andrews, B. Dowd, P. Siddons, A. Peskin, P. Spanne, and W. E. Soll, Developments in Synchrotron X-ray Microtomography with Applications to Flow in Porous Media, Proc. 1996 Annual Technical Conference and Exhibition, Denver, Colorado, October 6-9, 1996, Paper SPE 36531, 413-424 (1996)

M. E. Coles, R. D. Hazlett, P. Spanne, W. E. Soll, E. L. Muegge, and K. W. Jones, Pore Level Imaging of Fluid Transport Using Synchrotron X-ray Microtomography, J. Petroleum Science & Engineering 19:55-63 (1998a)

M. E. Coles, R. D. Hazlett, E. L. Muegge, K. W. Jones, B. Andrews, B. Dowd, P. Siddons, A. Peskin, P. Spanne, and W. E. Soll, Developments in Synchrotron X-Ray Microtomography with Applications to Flow in Porous Media, SPE Reservoir Evaluation & Engineering, 288-296 (August 1998b)

K. L. D'Amico, J. H. Dunsmuir, S. R. Ferguson, B. P. Flannery, and H. W. Deckman, The Exxon Microtomography Beam Line at the National Synchrotron Light Source, Rev. Sci. Instrum., 63:574-577 (1992)

J. S. Delaney, S. Bajt, S. R. Sutton, and M. D. Dyar, *In situ* Microanalysis of $Fe^{3+}/3Fe$ in Amphibole by X-ray Absorption Near Edge Structure (XANES) Spectroscopy, Mineral Spectroscopy, Special Publication No. 5, 165-171 (1996)

Jeremy S. Delaney, Steven R. Sutton, and M. Darby Dyar, Variable Oxidation States of Iron in Martian Meteorites, Lunar and Planetary Science XXIX, #1241 (CD-ROM), March (1998a)

Jeremy S. Delaney, M. Darby Dyar, Steven R. Sutton, and Sasa Bajt, Redox Ratios with Relevant Resolution: Solving an Old Problem Using the Synchrotron MicroXANES Probe, Geology 26:139-142 (1998b)

I. P. Dolbyna, A. V. Golubev, K. V. Zolotarev, V. A. Bobrov, and I. A. Kalugin, Scanning Synchrotron Radiation X-ray Fluorescence Trace Element Analysis of Microlayers of Fe-Mn Nodules: New Data on Ore Forming Processes in the Ocean. Nucl. Instrum. and Meth. in Phys. Res., A359:327-330 (1995)

B. A. Dowd, a. B. Andrews,R. B. Marr, D. P. Siddons, K. W. Jones, and A. M. Peskin, Advances in X-ray Computed Microtomography at the NSLS, Presented at 47th Annual Denver X-ray Conference, Colorado Spring, Colorado, August 3-7, 1998

James I. Drever, The Geochemistry of Natural Waters, 2nd edition, Prentice Hall, Englewood Cliffs, New Jersey, pp. 91-94 (1988)

European Synchrotron Radiation Facility. Highlights 1996/1997. X-Ray Tomography With Micrometer Spatial Resolution, p. 9; High-resolution Phase Contrast Microscopy with an X-ray Waveguide, p.10 (1997)

G. W. Grime and W. Davison, The Use of Nuclear Microprobe Techniques to Study the Chemistry of Lacustrine Sediments and Particles, Nucl. Instrum. Meth. in Phys. Res., B77:430-435 (1993)

R. D. Hazlett, Simulation of Capillary-Dominated Displacements in Microtomographic Images of Reservoir Rocks, Transport in Porous Media 20:21-35 (1995)

G. T. Herman, Image Reconstruction from Projections, The Fundamentals of Computerized Tomography, Academic Press, New York, 316 pp. (1980)

J. P. Hogan, R. A. Gonsalves, and A. S. Krieger, Fluorescent Computer Tomography: A Model for Correction of X-Ray Absorption, IEEE Trans. Nucl. Sci., 38:1721-1727 (1991)

John P. Hogan, Principles of Fluorescent Computed Tomography with Applications in Non-Destructive Testing, Ph.D. Thesis, Tufts University, May (1993)

G. P. Huffman, F. E. Huggins, A. A. Levasseur, J. F. Durant, F. W. Lytle, R. B. Greegor, and A. Mehta, Investigation of Atomic Structures of Calcium in Ash and Deposits Produced During the Combustion of Lignite and Bituminous Coal, Fuel 68:238-242 (1989)

G. E. Ice. Microbeam-Forming Methods for Synchrotron Radiation. X-ray Spectrometry 26:315 (1997)

T. Irifune, N. Nishiyama, K. Kuroda, T. Inoue, M. Isshiki, W. Utsumi, K. Funakoshi, S. Urakawa, T. Uchida, T. Katsura, and O. Ohtaka, The Postspinel Phase Boundary in Mg_2SiO_4 Determined by in Situ x-ray Diffraction, Science 279:1698-1700 (1998)

Janssens et al., private communication (1998)

Robert A. Johns, John S. Steude, Louis M. Castanier, and Paul V. Roberts, Nondestructive Measurements of Fracture Aperture in Crystalline Rock Cores Using X Ray Computed Tomography, Journal of Geophysical Research 98: 1889-1900 (1993)

K. W. Jones, Synchrotron Radiation-Induced X-ray Emission, in Handbook of X-ray Spectrometry, René E. Van Grieken and Andrzej A. Markowicz, editors, Marcel Dekker, New York, pages 411-452, (1992)

K. W. Jones, P. Spanne, S. W. Webb, W. C. Conner, R. A. Beyerlein, W. J. Reagan, and F. M. Dautzenberg, Catalyst Analysis Using Synchrotron X-ray Microscopy, Nucl. Instrum. Meth. in Phys. Res. B56/57:427-432 (1991)

K. W. Jones, C. Riekel, P. Engstrom, J. Sweeny, and D. Heinz, private communication (1996)

Apostolos Kantzas, Investigation of Physical Properties of Porous Rocks and Fluid Flow Phenomena in Porous Media using Computer Assisted Tomography, In Situ 14:77-132, (1990)

J. H. Kinney and M. C. Nichols, X-ray Tomographic Microscopy (XTM) Using Synchrotron Radiation. Ann. Rev. Mater. Sci., 22:121-152 (1992)

A. Koch, C. Raven, P. Spanne, and A. Snigirev, X-ray Imaging with Submicrometer Resolution Employing Transparent Luminescent Screens, J. Optical Society of America, A, Optics and Image Science, 15:1940 (1998)

Allan Kolker and Chen-Lin Chou, Cleat-Filling Calcite in Illinois Basin Coals: Trace-Element Evidence for Meteoric Fluid Migration in a Coal Basin, J. of Geology 102:111-116 (1994)

H. Kucha, Przyblowicz, Lankosz, M. van Langevelde, and K. Traxel, BPMA, Micro-PIXE, Synchrotron Microprobe, and TEM Study of Visible and Invisible Accumulations of AU and PGB in Black Shale and Organic Matri, Kupferschiefer, Poland, Mineral Mag., 57:103-112 (1993)

S. Lagomarsino, A. Cedola, P. Cloetens, S. Di Fonzo, W. Jark, G. Soullié, J, and C. Riekel, Phase Contrast Hard X-ray Microscopy with Submicron Resolution, Appl. Phys. Letters 71:2557-2559 (1997)

W. B. Lindquist, S.-M. Lee, D. A. Coker, K. W. Jones, and P. Spanne, Medial Axis Analysis of Void Structure in Three-Dimensional Tomographic Images of Porous Media, J. of Geophys. Res. 101:8297-8310 (1996)

J. A. Mavrogenes, R. J. Bodnar, A. J. Anderson, S. Bajt, S. R. Sutton, M. L. Rivers, Assessment of the Uncertainties and Limitations of Quantitative Elemental Analysis of Individual Fluid Inclusions Using Synchrotron X-ray Fluorescence (SXRF), Geochim. Cosmochim. Acta 59:3987-3996 (1995)

National Research Council, Committee on Contaminated Marine Sediment, Marine Board, Commission on Engineering and Technical Systems, Contaminated Sediments in Ports and Waterways, Cleanup Strategies and Technologies, National Academy Press, Washington, DC (1997)

C. R. Olsen, N. H. Cutshall, and L. L. Larsen, Pollutant-Particle Associations and Dynamics in Coastal Marine Environments: A Review, Marine Chemistry 11:501-533 (1982)

Reinhard Pahl and Donald H. Bilderback, Development of Capillary Optics for Microbeam Applications with Synchrotron Radiation. Society of Photo-Optical Instrumentation Engineers. 2805:202-211 (1996)

J. J. Pluth, J. V. Smith, D. Y. Pushcharovsky, E. I. Semenov, A. Bram, C. Riekel, H.-P. Weber, and R. W. Broach, Third-generation Synchrotron X-ray Diffraction of 6-μm Crystal of Raite, $\approx Na_3Mn_3Ti_{0.25}Si_8O_{20}(OH)_2 \cdot 10H_2O$ Opens Up New Chemistry and Physics of Low-Temperature Minerals, Proceedings of the National Academy of Sciences (USA) 94:12263-12267 (1997)

A. R. Pratt, C. M. Huctwith, P. A. W. van der Heide, and N. S. McIntyre, Quantitative SIMS Analysis of Trace Au in Pyrite Using the Infinite Velocity (IV) Method, J. Geochemical Exploration 60:241-247 (1998)

C. Raven, A. Koch, and A. Snigirev, CellVision 4:157 (1997)

M. L. Rivers, T. S. Duffy, Y. Wang, P. J. Eng, S. R. Sutton, and G. Shen, A New Facility for High-Pressure Research at the Advanced Photon Source, in Properties of Earth and Planetary Materials at High Pressure and Temperature, M. H. Manghnani and T. Yagi, editors, American Geophysical Monograph Series, Volume 101, American Geophysical Union, Washington, DC (1998)

R. M. S. Schofield and H. W. Lefevre, PIXE-STIM Microtomography: Zinc and Manganese Concentrations in a Scorpion Stinger. Nucl. Instrum. and Meth. in Phys. Res. B72:104-110 (1992)

L. M. Schwartz, F. Auzerais, J. Dunsmuir, N. Martys, D. P. Bentz, and S. Torquato, Transport and Diffusion in Three Dimensional Composite Media, Physica A 207:28-36 (1994)

E. M Scott and R. A. Williams, editors, Frontiers in Industrial Process Tomography, Engineering Foundation , New York, NY, 346 pp. (1995)

Naresh Shah, Gerald P. Huffman, and Frank E. Huggins, Determination of the Forms and Concentration of Critical Trace elements in Coal by XAFS Spectroscopy, in Proceedings of the Tenth International Pittsburgh Coal Conference, Coal, Energy and the Environment, editors, Shiao-Hung Chiang, September 20-24, 1993, Pittsburgh, Pennsylvania, 320-325 (1993)

Naresh J. Shah, Zhaok, K. R. P. M. Rao, F. E. Huggins and G. P. Huffman, *In-situ* XAFS Spectroscopic Studies of DCL Catalysts, in Coal Science, Proceedings of the Eighth International Conference on Coal Science, J. A. Pajares and J. M. D. Tascón, editors,1279-1282, Elsevier Science, New York (1995)

F. J. Simons, F. Verhelst, and R. Swennen, Quantitative Characterization of Coal by Means of Microfocal X-ray Computed Microtomography of (CMT) and Color Image Analysis (CIA), Intern. J. of Coal Geology 34:69 (1998)

J. V. Smith, Tutorial Review: Synchrotron x-ray Sources: Instrumental Characteristics. New Applications in Microanalysis, Tomorgraphy, Absorption Spectroscopy and Diffraction, The Analyst 120:1231-1245 (1995)

J. V. Smith and M. L. Rivers, in Microprobe Techniques in the Earth Sciences, P. Potts, J. F. W. Bowles, S. J. B. Reed, and M. R. Cave, editors, Chapter 5, 163-233, Chapman and Hall, London (1995)

Sheng-Rong Song and K. W. Jones, Elemental Analysis of Contaminated Sediments from Harbor of NY/NJ and Hamburg Using Synchrotron Radiation-Induced X-Ray Emission (SRIXE), presented at 1997 Spring Meeting of the American Geophysical Union, Baltimore, Maryland, May 27-30, 1997

P. Spanne, K. W. Jones, L. D. Prunty, and S. H. Anderson, Potential Applications of Synchrotron Computed Microtomography to Soil Science, in Tomography of Soil-Water Root Processes, Stephen H. Anderson and Jan Hopmans, editors, Soil Science Society of America, SSSA Special Publication Number 36, Madison, Wisconsin, 43-57 (1994a)

P. Spanne, J. F. Thovert, C. J. Jacquin, W. B. Lindquist, K. W. Jones, and P. M. Adler, Synchrotron Computed Microtomography of Porous Media: Topology and Transports, Phys. Rev. Lett. 73:2001-2004 (1994b)

D. J. Thiel, D. H. Bilderback, A. Lewis, E. A. Stern, and T. Rich, Guiding and Concentrating Hard X-rays by Using a Flexible Hollow-Core Tapered Glass Fiber, Applied Optics 31: 987-992 (1992)

Sz. B. Török, K. W. Jones, and C. Tuniz, Characterization of Geological Materials Using Ion and Photon Beams, in Nuclear Methods in Mineralogy and Geology, Techniques and Applications, Attila Vértes, Sándor Nagy, and Károly Süvegh, editors, 217-249, Plenum Press, New York (1998)

U. S. Environmental Protection Agency, EPA's Contaminated Sediment Management Strategy. Washington, DC (1998)

M. A. Vairavamurthy, S. Wang, B. Khandelwal, B. Manowitz, T. Ferdelman, and H. Fossing, sulfur Transformations in Early Diagenetic Sediments from the Bay of Concepcion, Off Chile, in ACS Symposium Series No. 612, Geochemical Transformations of Sedimentary Sulfur, M. A. Vairavamurthy and M. A. A. Schoonens, editors, 38-58, American Chemical Society, Washington, DC (1995)

Murthy A. Vairavamurthy, Dusan Maletic, Shenkhe Wang, Bernard Manowitz, Timothy Eglinton, and Timothy Lyons, Characterization of Sulfur-Containing Functional Groups in Sedimentary Humic Substances by X-Ray Absorption Near-Edge Structure Spectroscopy, Energy & Fuels, 11:546-553 (1997)

F. Verhelst, P. David, W. Fermont, L. Jegers, and A. Vervoort, Correlation of 3D-Computerized Tomographic Scans and 2D-Colour Image Analysis of Westphalian Coal by Means of Multivariate Statistics, Int. Journ. of Coal Geology 29:1-21 (1996)

S. Y. Wang, Y. B. Huang, V. Pereira, and C. C. Gryte, Application of Computed Tomography to Oil Recovery From Porous Media, Applied Optics 24:4021-4027 (1985)

FIGURE CAPTIONS

Figure 1. X-ray fluxes produced at the Brookhaven National Synchrotron Light Source and the Argonne Advanced Photon Source. (Courtesy M. L. Rivers, University of Chicago).

Figure 2. Photograph of the University of Chicago Center for Advanced Radiation Sources x-ray fluorescence beam line at the Argonne Advanced Photon Source. (Photograph courtesy of S. R. Sutton, University of Chicago).

Figure 3. Comparison of $Fe^{3+}/\Sigma Fe$ ratio determined using synchrotron micro-XANES results with those obtained using wet chemistry (Delaney et al., 1998a).

Figure 4. SRIXE spectra obtained for pyrite (4a) and matrix material (4b) in a gold ore sample. Gold was found in the matrix material (Chen et al., 1987).

Figure 5. Correlation of Ga and Au concentrations with the total W and Ta concentration in a specimen of ore containing Au (Basto et al., 1995).

Figure 6. Variation of Mn, Ni, Cu, Fe, Sr, and Zr found in a radial scan across a Fe-Mn nodule. The existence of differences in the concentrations reflect different conditions at the time of formation of the nodule. (Dolbyna et al., 1995).

Figure 7. Dependence of the concentration of dissolved Fe on depth in the region just below the sediment-water interface in a fresh-water lake. The measurements were made using Rutherford backscattering. (Grime and Davison, 1993).

Figure 8. SRIXE measurement of dependence of lead concentrations as a function of particle size for sediments taken from Newtown Creek in Brooklyn/Queens, New York. (Song and Jones,1997).

Figure 9. SRIXE measurement of the radial dependence of lead in a sediment particle from Newtown Creek. The step size used in the scan was 100 μm. (Song and Jones, 1997).

Figure 10. SRIXE spectra of rare-earth elements in an ore sample and a standard demonstrating the usefulness of SRIXE for studying rare-earth elements in trace quantities and high-spatial resolution (Chen et al., 1993).

Figure 11. Two dimensional maps of Fe, Mn, and Sr in a calcite with a pixel size of 25 μm obtained using SRIXE. The maps offer a clear picture of the zoning occurring in this specimen (Kolker and Chou, 1994).

Figure 12. Laue-diffraction spectrum obtained with a 13 keV x-ray beam incident on a specimen of silicate perovskite using an image-plate x-ray detector. (Jones et al., 1996).

Figure 13. Laue-diffraction spectrum obtained with a 13-keV x-ray beam incident on a specimen of silicate perovskite using a CCD x-ray detector. (Jones et al., 1996).

Figure 14. Phase diagram for Fe showing need to obtain experimental data at high pressures. (Anderson, 1997).

Figure 15. Diffraction spectra obtained as a function of pressure showing evidence for a phase transformation in Fe. (Andrault et al., 1997).

Figure 16. X-ray diffraction spectra obtained for olivine at different temperatures and pressures. The spectrum obtained from the native olivine material is displayed in (A). When the pressure is raised to 24 GPa and the temperature to 1100 °C a spinel phase is found as shown in (B). As the temperature is increased further, evidence is found for perovskite and perclase phases as is seen in (C). A reduction in the temperature then brings about the partial conversion of these phases to the spinel phase (D). (Irifune et al., 1998).

Figure 17. Schematic diagram showing the equipment used for computed microtomography experiments at the NSLS X27A beam line. (Dowd et al., 1998).

Figure 18. Tomographic volumes and sections showing pore spaces in a rock following displacement of oil (white) by brine (black) in a sandstone (grey). (Coles et al., 1998b).

Figure 19. Tomographic volume showing the distribution of water in the sandstone (Coles et al., 1998b).

Figure 20. Comparison of experimental measurements of the measured water distribution found for four sections with theoretical calculations based on the lattice Boltzmann model developed at Los Alamos. (Coles et al., 1998b).

Figure 21. Tomographic volume obtained for a North Sea Brent sandstone using the equipment described by Dowd et al. (1998). The voxel size is 2.7 μm. (Coles et al., 1998b).

Figure 22. Distribution of S, Ca, V, Cr, Fe, Ni, Cu, Zn, and Mo in a section of a fly ash particle measured using fluorescent tomography (Janssens et al., 1998).

Figure 23. Xanes spectra for sediments and humic acids obtained from Shelter Island, New York salt marsh, Florida Bay, and the Peru margin. (Vairavamurthy et al., 1997).

Figure 24. Xanes calibration spectra for model compounds. These spectra for both organic and inorgainic sulphur compounds can be used in the analysis of XANES spectra obtained for the humic acid and sediment samples. (Vairavamurthy et al., 1995).

Figure 25. Nonlinear least-squares fits of model compound XANES spectra to Shelter Island, New York salt marsh sediment data. (Vairavamurthy et al., 1997).

Figure 26. XANES spectra for coal samples taken from different mine locations. (Shah et al., 1993).

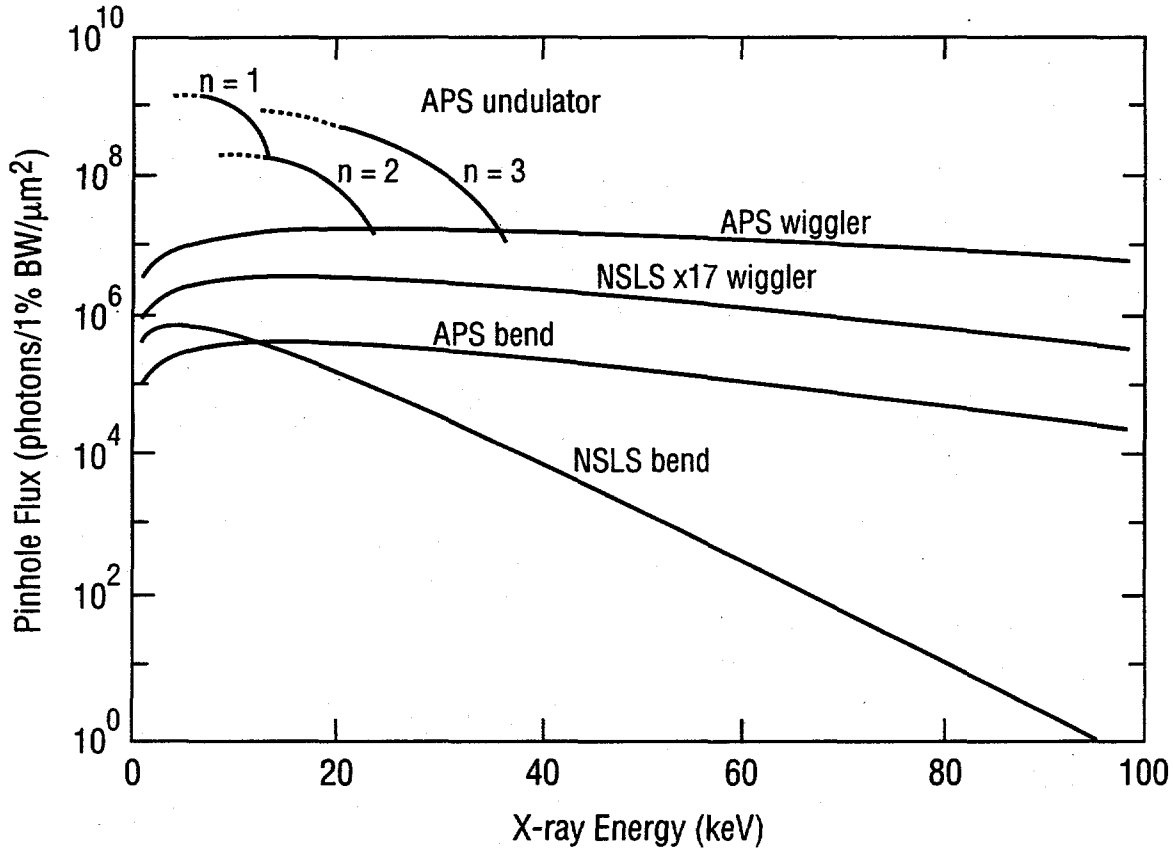
Pinhole Flux (photons/1% BW/μm²)
10¹⁰
10⁸
10⁶
10⁴
10²
10⁰
n = 1
n = 2
n = 3
APS undulator
APS wiggler
NSLS x17 wiggler
APS bend
NSLS bend
0
20
40
60
80
100
X-ray Energy (keV)

Figure 1

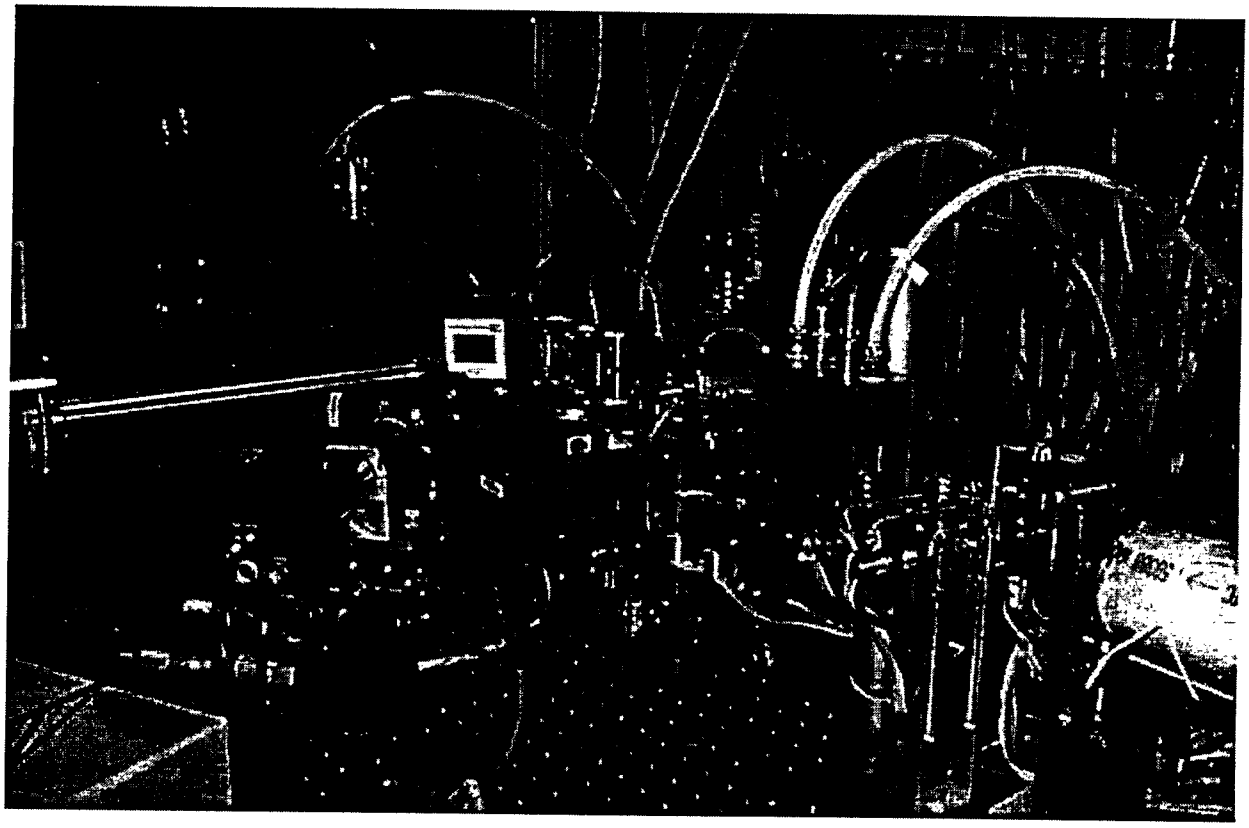

Figure 2

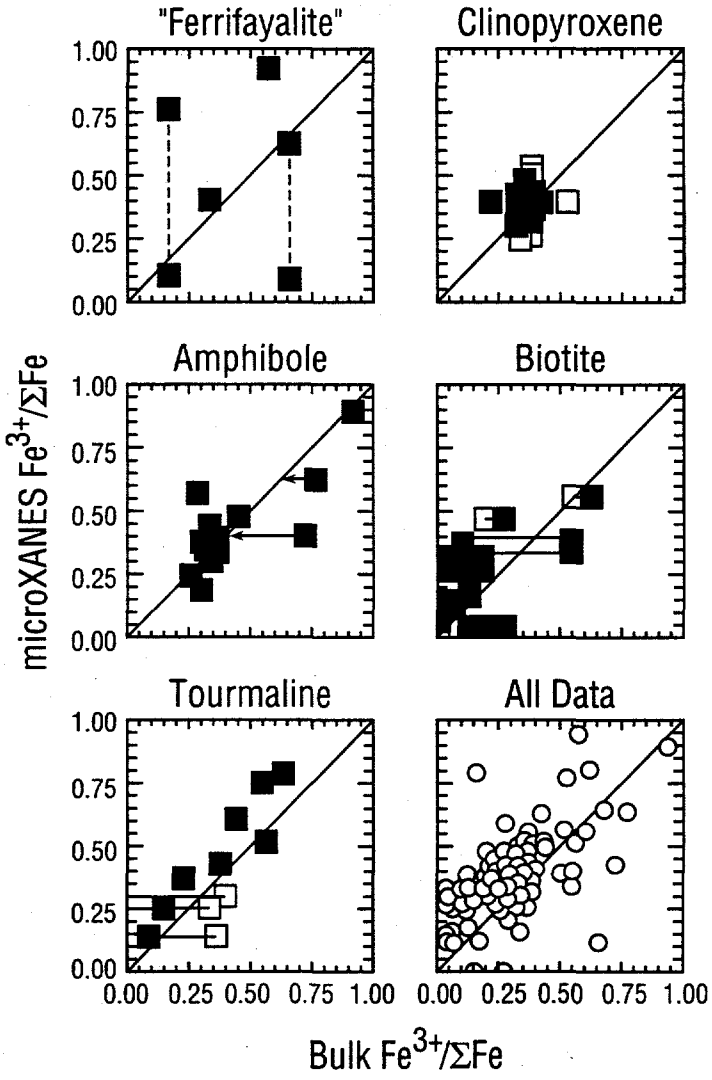
"Ferrifayalite"
Clinopyroxene
Amphibole
Biotite
Tourmaline
All Data
1.00
0.75
0.50
0.25
0.00
0.00 0.25 0.50 0.75 1.00
microXANES Fe3+/ΣFe
Bulk Fe3+/ΣFe

Figure 3

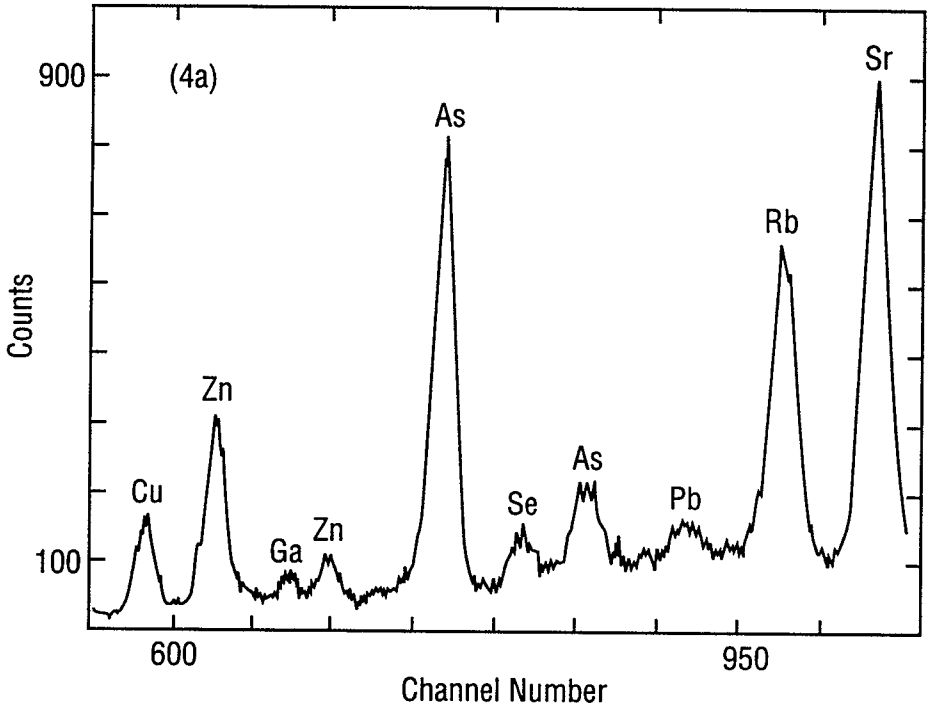
900
100
Counts
(4a)
Cu
Zn
Ga
Zn
As
Se
As
Pb
Rb
Sr
600
950
Channel Number

Figure 4a

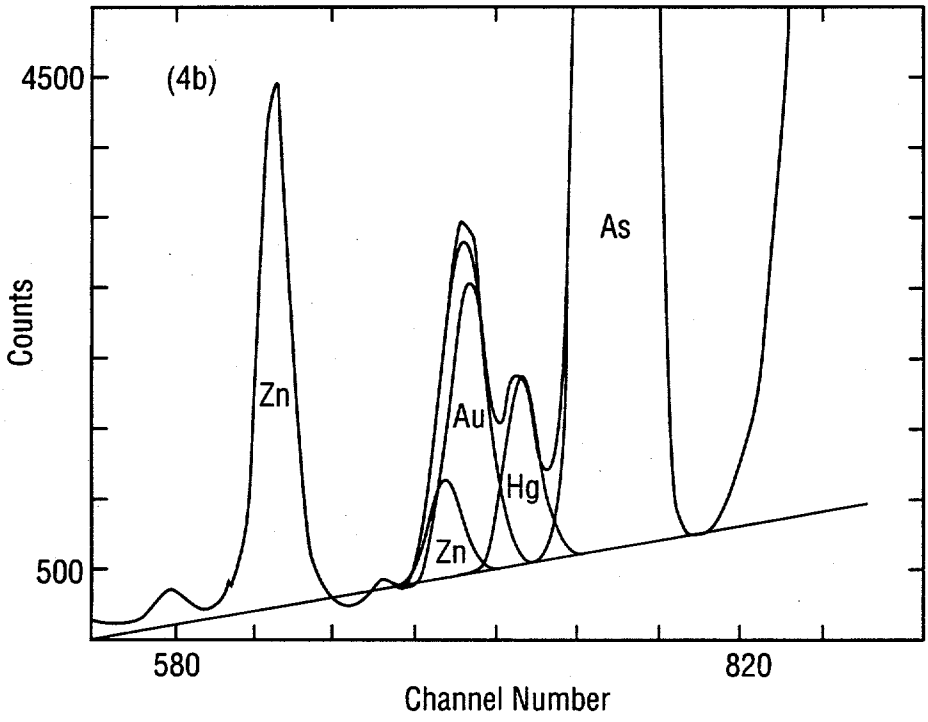

Figure 4b

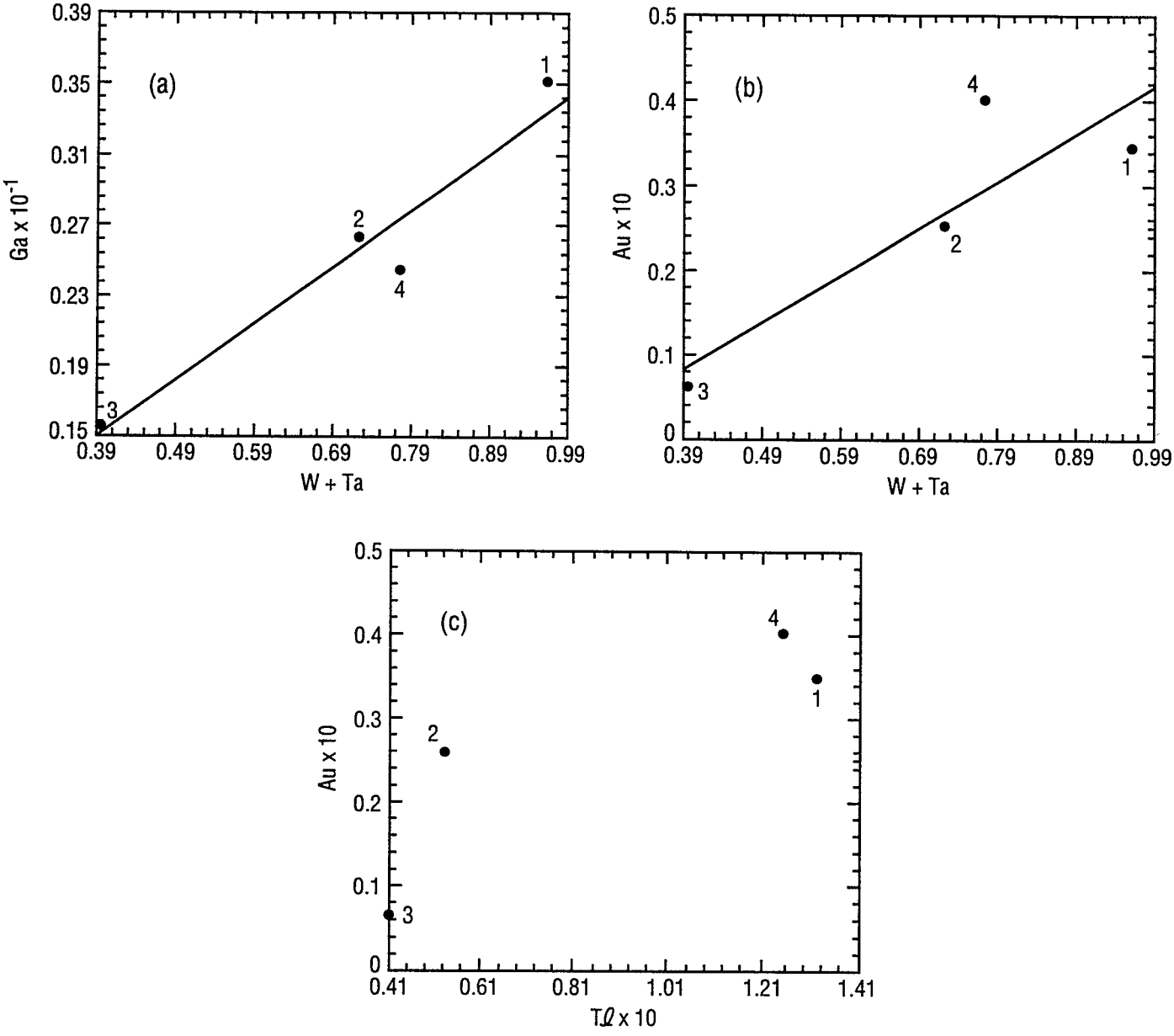
(a)
Ga x 10⁻¹
W + Ta
0.39
0.35
0.31
0.27
0.23
0.19
0.15
0.39
0.49
0.59
0.69
0.79
0.89
0.99
1
2
3
4
(b)
Au x 10
W + Ta
0.5
0.4
0.3
0.2
0.1
0
(c)
Tℓ x 10
0.41
0.61
0.81
1.01
1.21
1.41

Figure 5

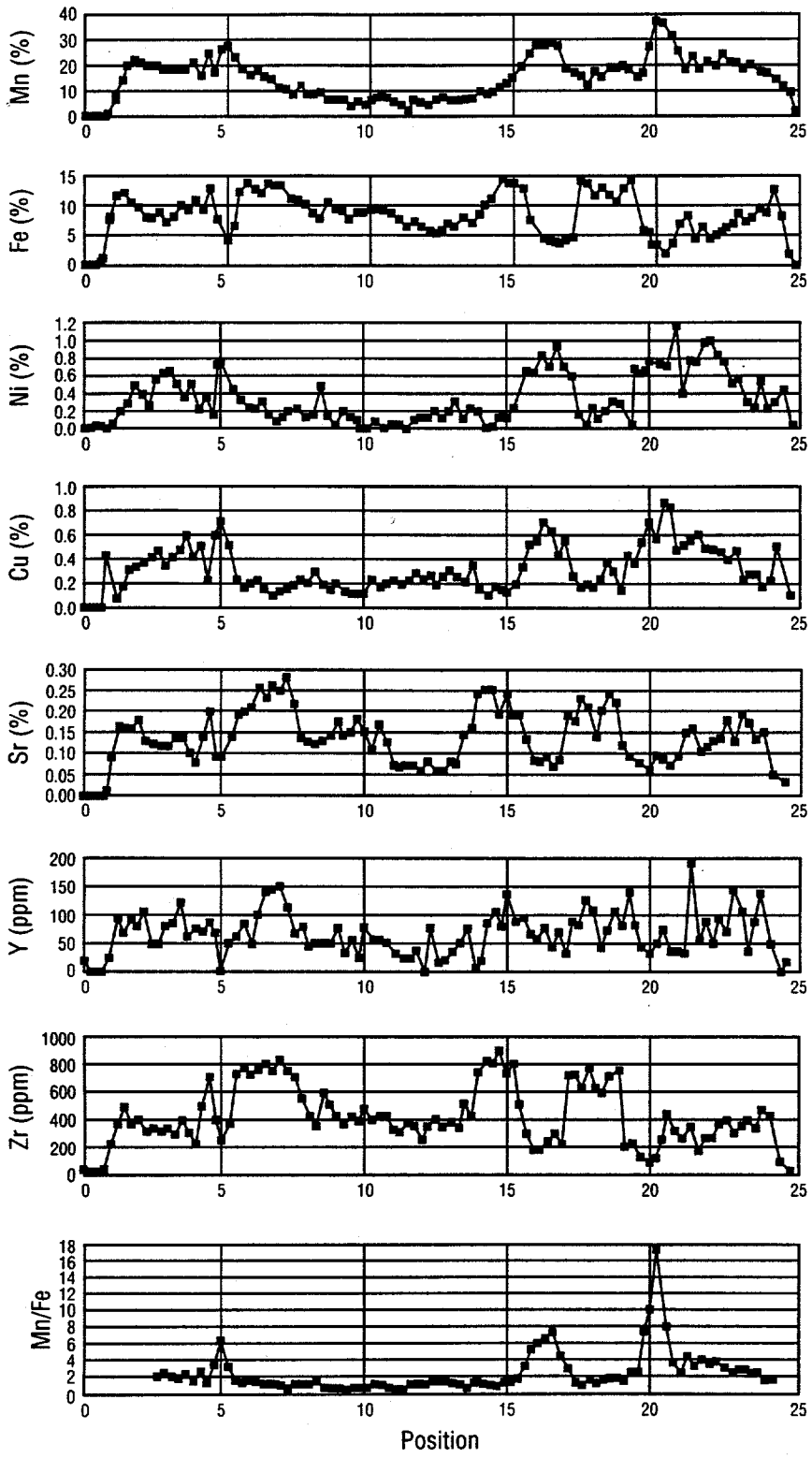

Figure 6

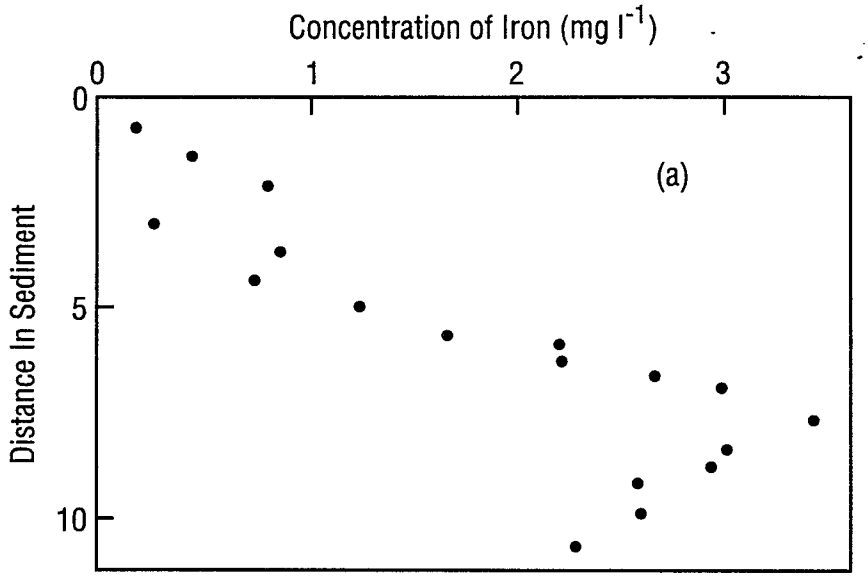
Concentration of Iron (mg l-1)
0
1
2
3
0
5
10
Distance In Sediment
(a)

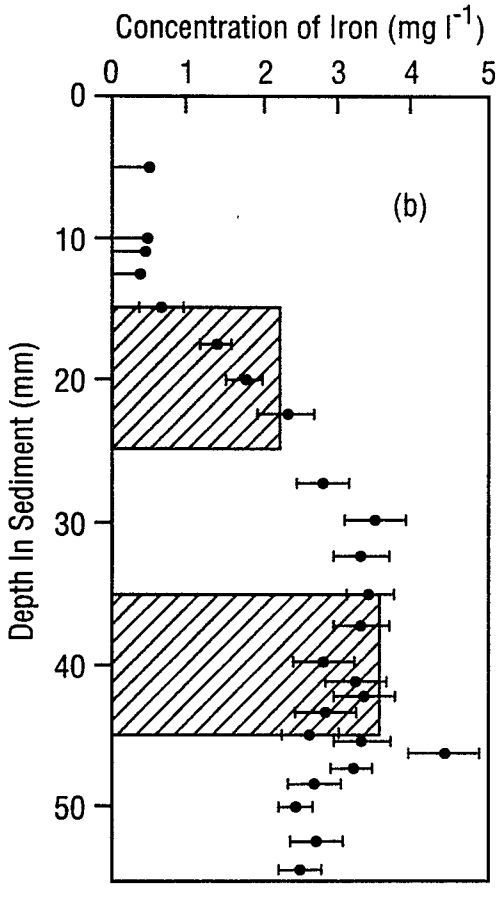
Concentration of Iron (mg l-1)
0
1
2
3
4
5
0
10
20
30
40
50
Depth In Sediment (mm)
(b)

Figure 7

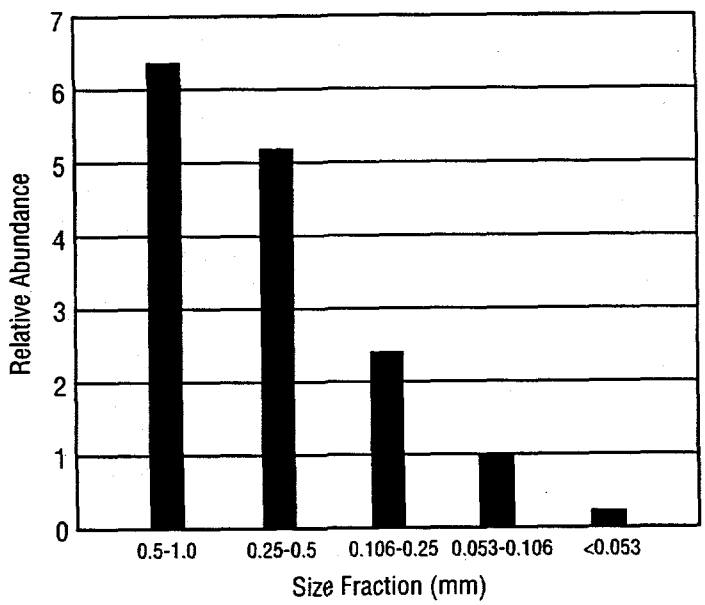
7
6
5
4
3
2
1
0
Relative Abundance
0.5-1.0
0.25-0.5
0.106-0.25
0.053-0.106
<0.053
Size Fraction (mm)

Figure 8

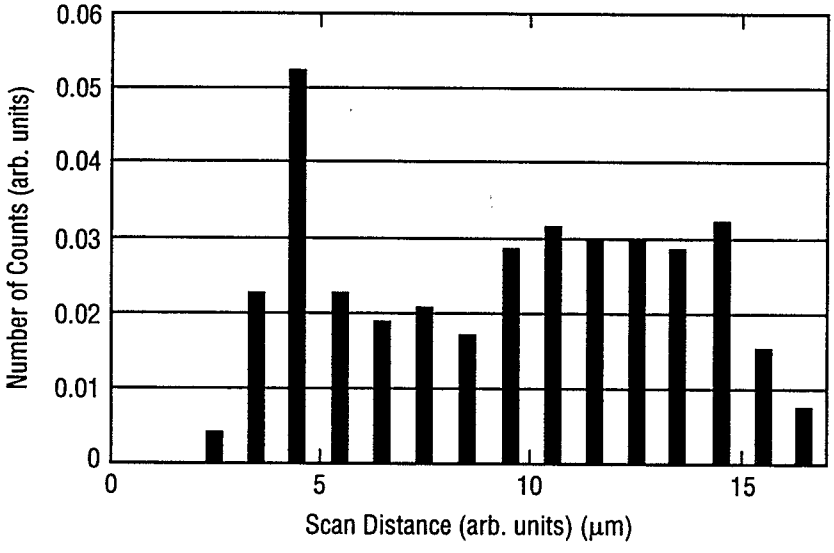
0.06
0.05
0.04
0.03
0.02
0.01
0
Number of Counts (arb. units)
0
5
10
15
Scan Distance (arb. units) (μm)

Figure 9

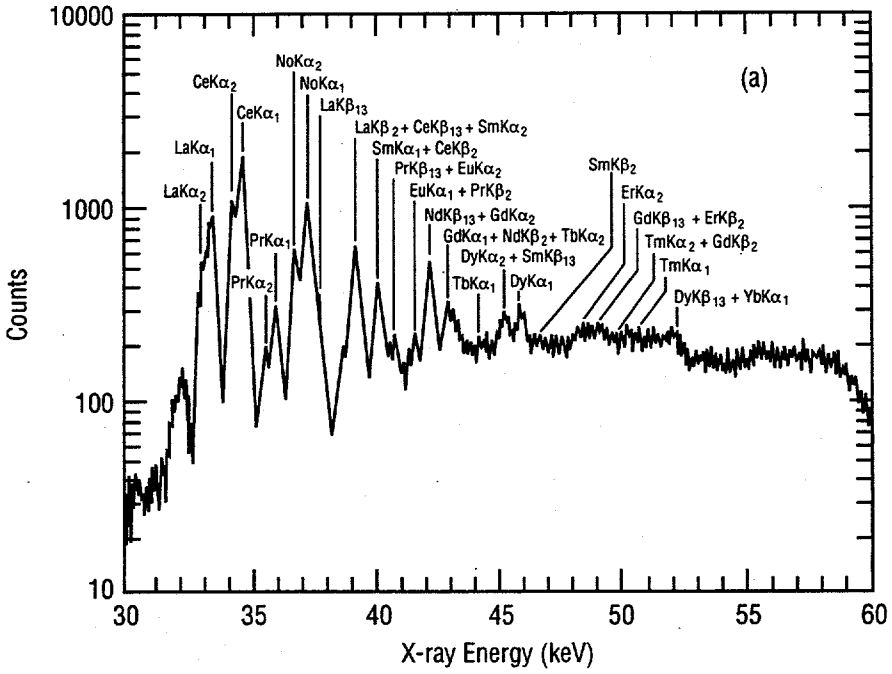
10000
1000
100
10
Counts
(a)
LaKα2
LaKα1
CeKα2
CeKα1
PrKα2
PrKα1
NoKα2
NoKα1
LaKβ13
LaKβ2 + CeKβ13 + SmKα2
SmKα1 + CeKβ2
PrKβ13 + EuKα2
EuKα1 + PrKβ2
NdKβ13 + GdKα2
GdKα1 + NdKβ2 + TbKα2
DyKα2 + SmKβ13
TbKα1
DyKα1
SmKβ2
ErKα2
GdKβ13 + ErKβ2
TmKα2 + GdKβ2
TmKα1
DyKβ13 + YbKα1
30
35
40
45
50
55
60
X-ray Energy (keV)

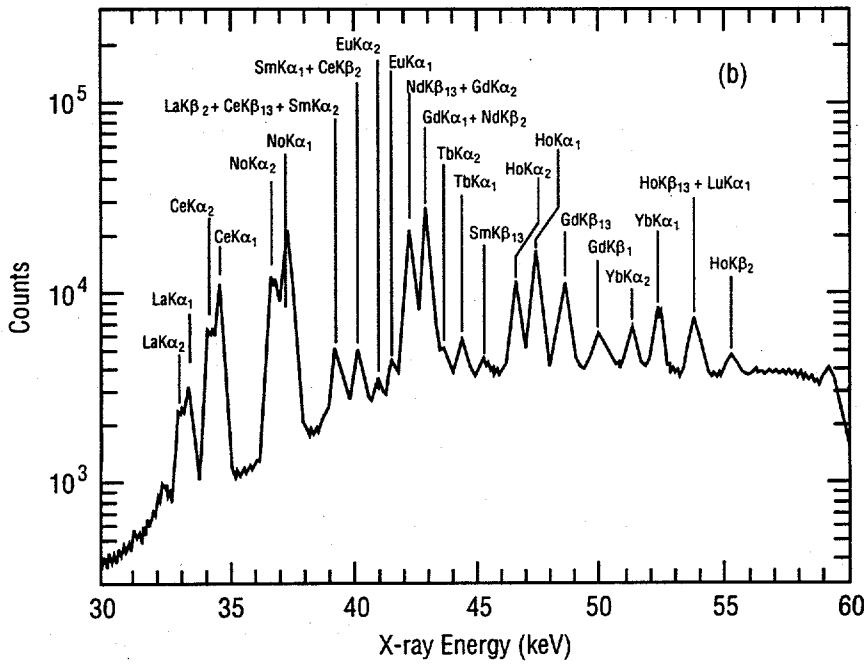
10^5
10^4
10^3
Counts
(b)
LaKα2
LaKα1
CeKα2
CeKα1
NoKα2
NoKα1
LaKβ2 + CeKβ13 + SmKα2
SmKα1 + CeKβ2
EuKα2
EuKα1
NdKβ13 + GdKα2
GdKα1 + NdKβ2
TbKα2
TbKα1
SmKβ13
HoKα1
HoKα2
GdKβ13
GdKβ1
YbKα2
YbKα1
HoKβ13 + LuKα1
HoKβ2
30
35
40
45
50
55
60
X-ray Energy (keV)

Figure 10

Figure 11

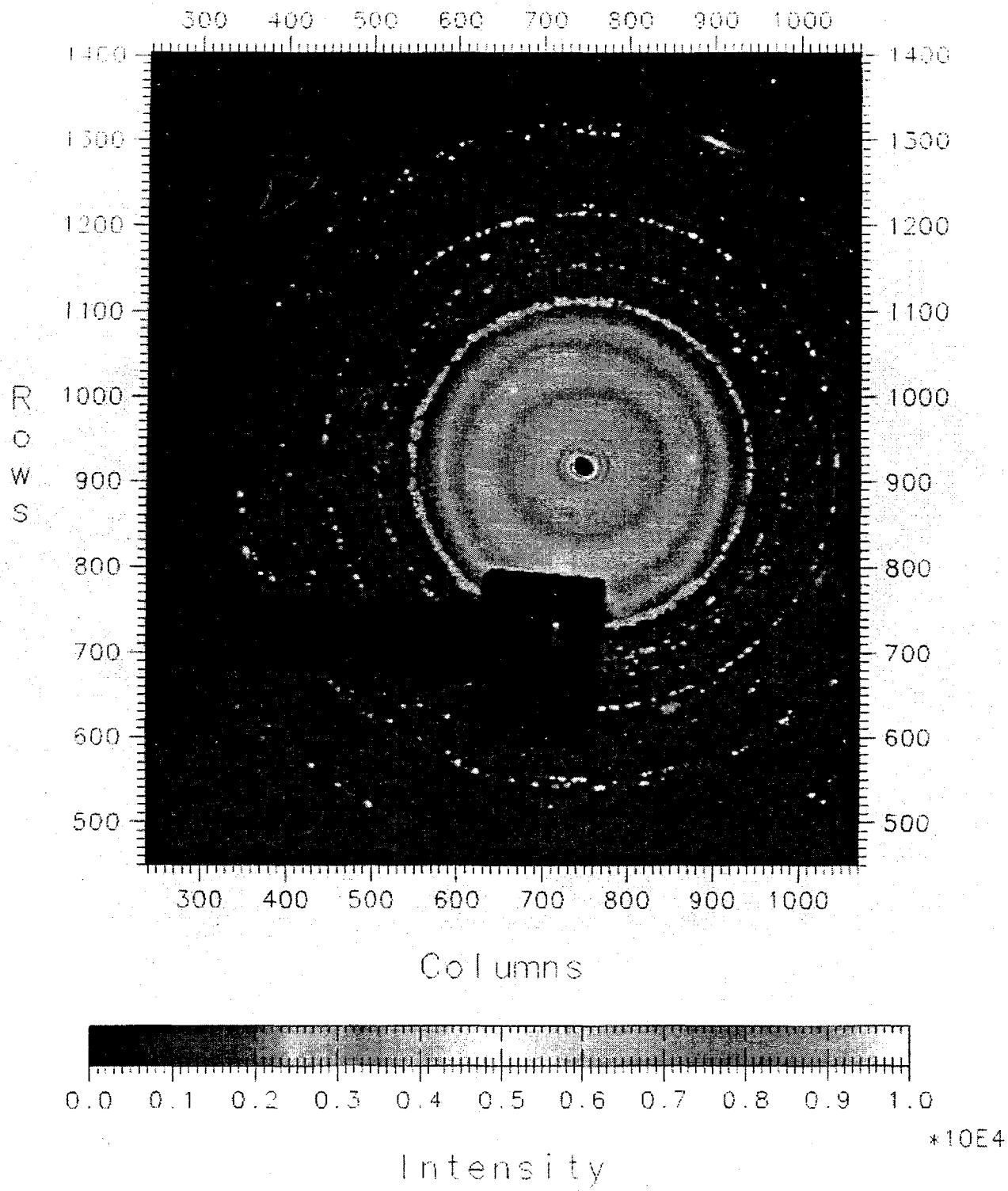
300 400 500 600 700 800 900 1000
1400
1300
1200
1100
1000
900
800
700
600
500
ROWS
Columns
0.0 0.1 0.2 0.3 0.4 0.5 0.6 0.7 0.8 0.9 1.0
*10E4
Intensity

Figure 12

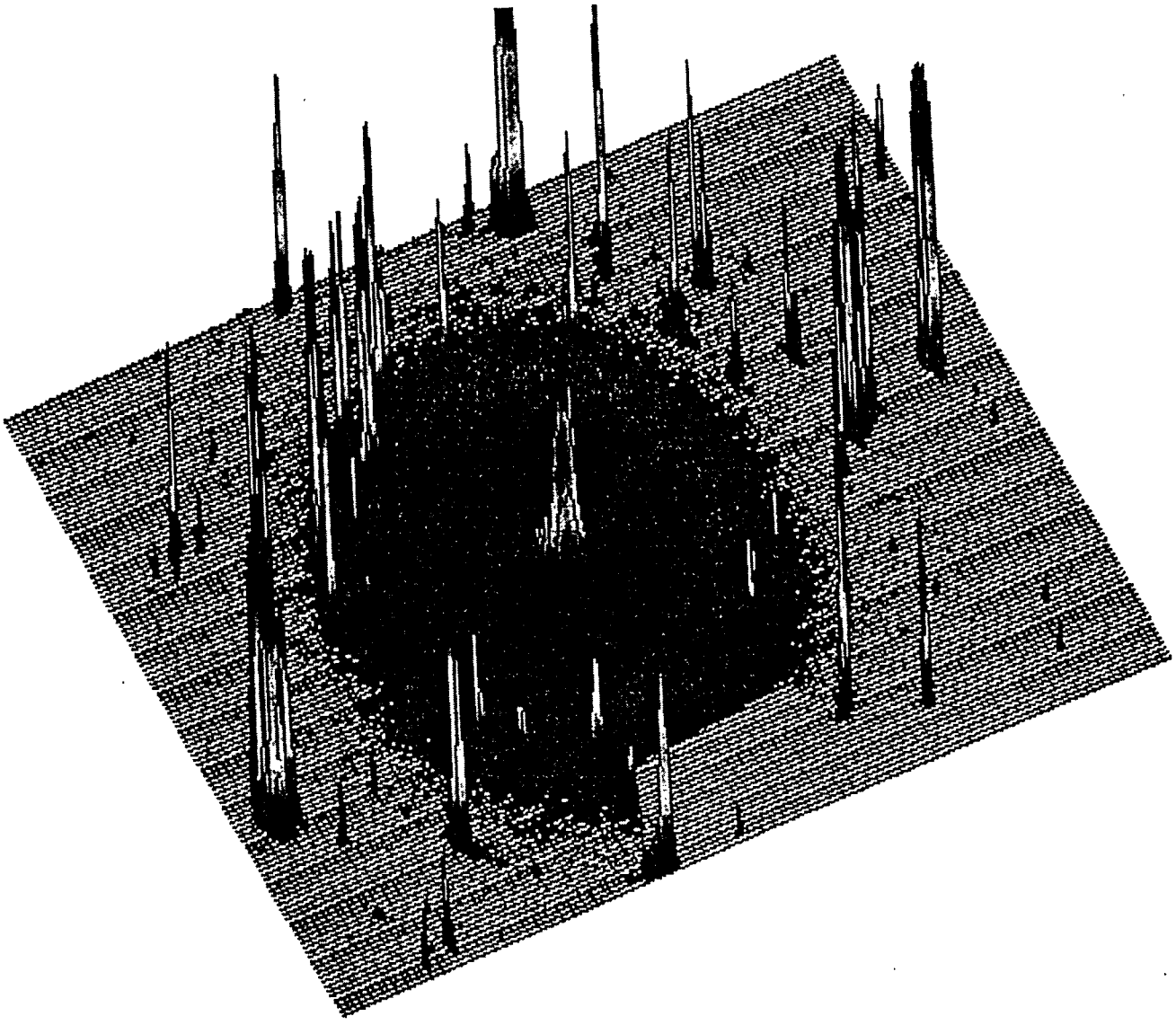

Figure 13

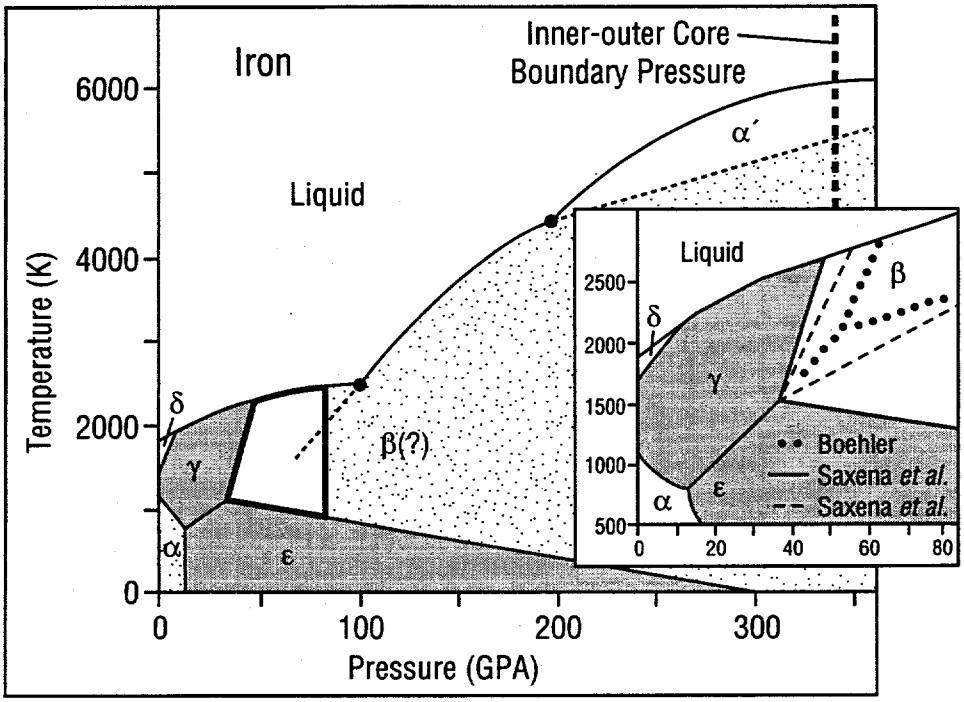
Iron
Inner-outer Core
Boundary Pressure
Liquid
α′
δ
γ
α
ε
β(?)
Temperature (K)
Pressure (GPA)
6000
4000
2000
0
0
100
200
300
Liquid
β
δ
γ
α
ε
2500
2000
1500
1000
500
0
20
40
60
80
Boehler
Saxena et al.
Saxena et al.

Figure 14

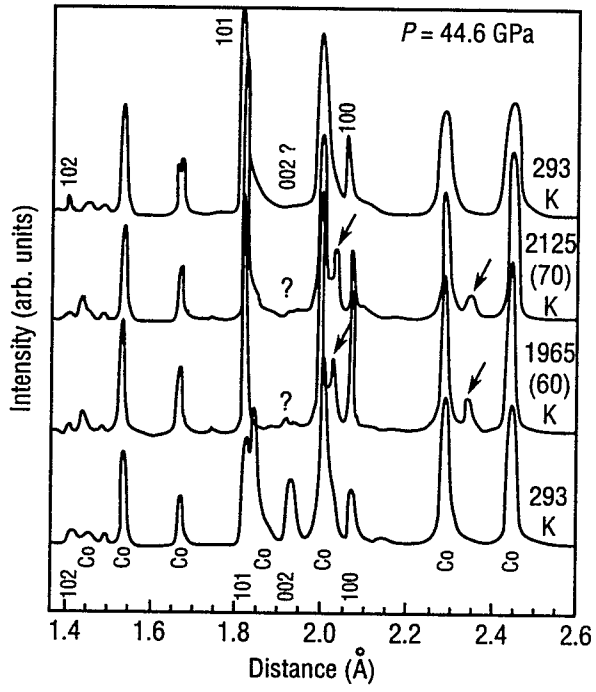
P = 44.6 GPa
101
100
102
002 ?
293 K
2125 (70) K
1965 (60) K
293 K
?
?
Co
Intensity (arb. units)
1.4
1.6
1.8
2.0
2.2
2.4
2.6
Distance (Å)

Figure 15

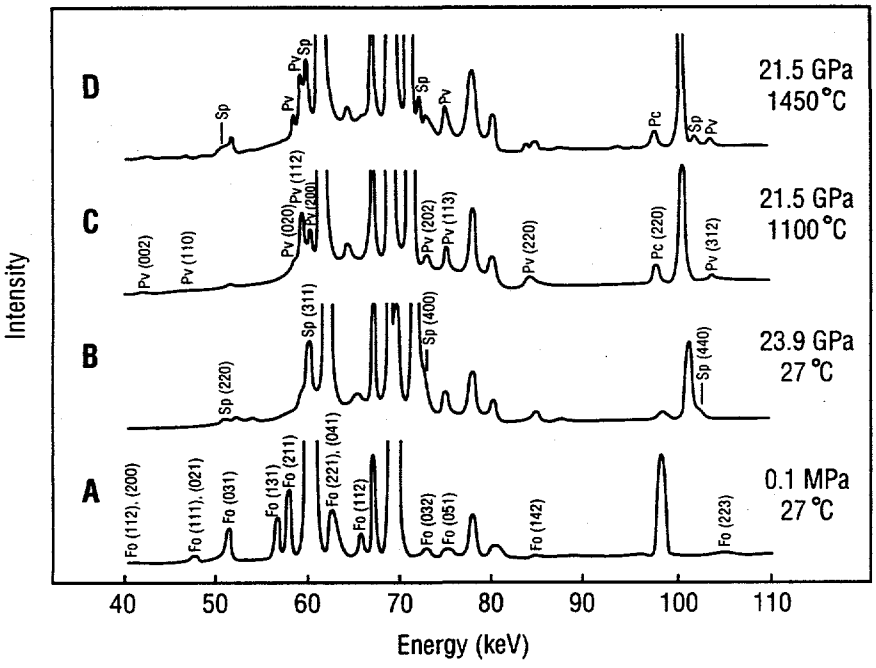
D
21.5 GPa
1450°C
Sp
Pv
Pv
Sp
Sp
Pv
Pc
Sp
Pv
C
21.5 GPa
1100°C
Pv (002)
Pv (110)
Pv (020)
Pv (112)
Fx (200)
Pv (202)
Pv (113)
Pv (220)
Pc (220)
Pv (312)
B
23.9 GPa
27 °C
Sp (220)
Sp (311)
Sp (400)
Sp (440)
A
0.1 MPa
27 °C
Fo (112), (200)
Fo (111), (021)
Fo (031)
Fo (131)
Fo (211)
Fo (221), (041)
Fo (112)
Fo (032)
Fo (051)
Fo (142)
Fo (223)
Intensity
40
50
60
70
80
90
100
110
Energy (keV)

Figure 16

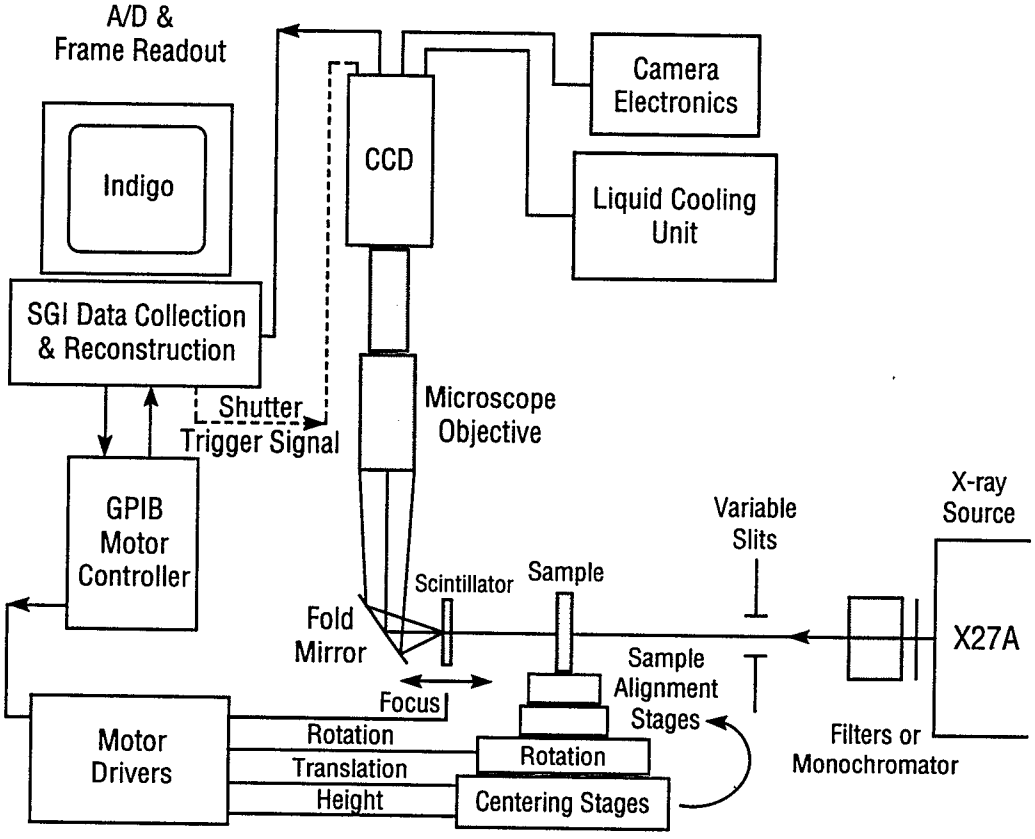
A/D &
Frame Readout
Indigo
SGI Data Collection
& Reconstruction
CCD
Camera
Electronics
Liquid Cooling
Unit
Shutter
Trigger Signal
Microscope
Objective
GPIB
Motor
Controller
X-ray
Source
Variable
Slits
Scintillator
Sample
Fold
Mirror
X27A
Sample
Alignment
Stages
Focus
Motor
Drivers
Rotation
Translation
Height
Rotation
Centering Stages
Filters or
Monochromator

Figure 17

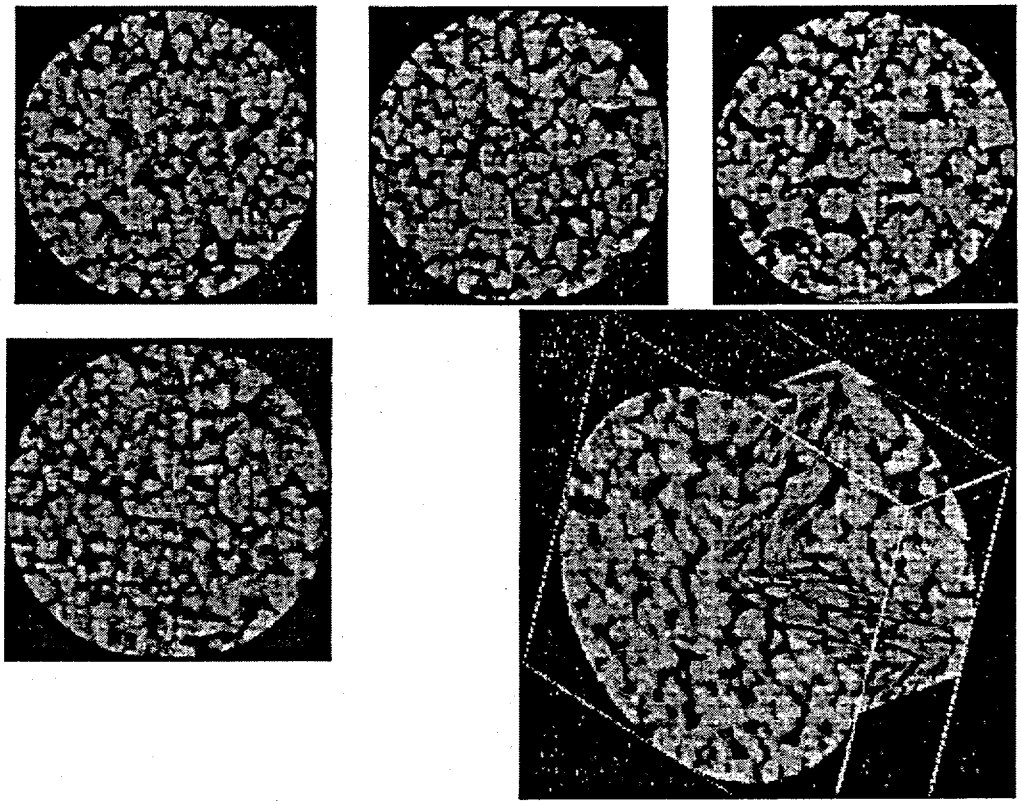

Figure 18

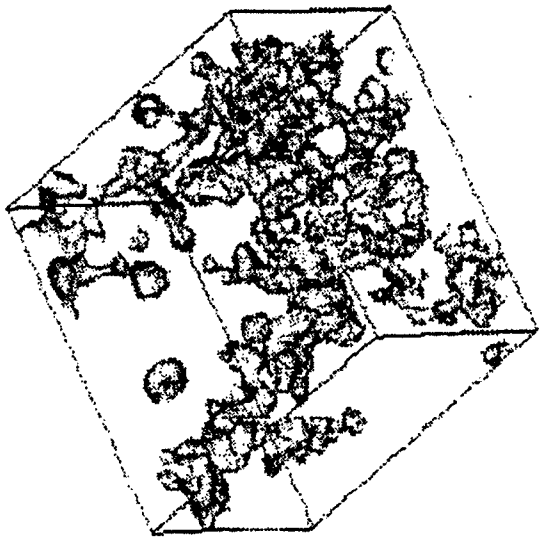

Figure 19

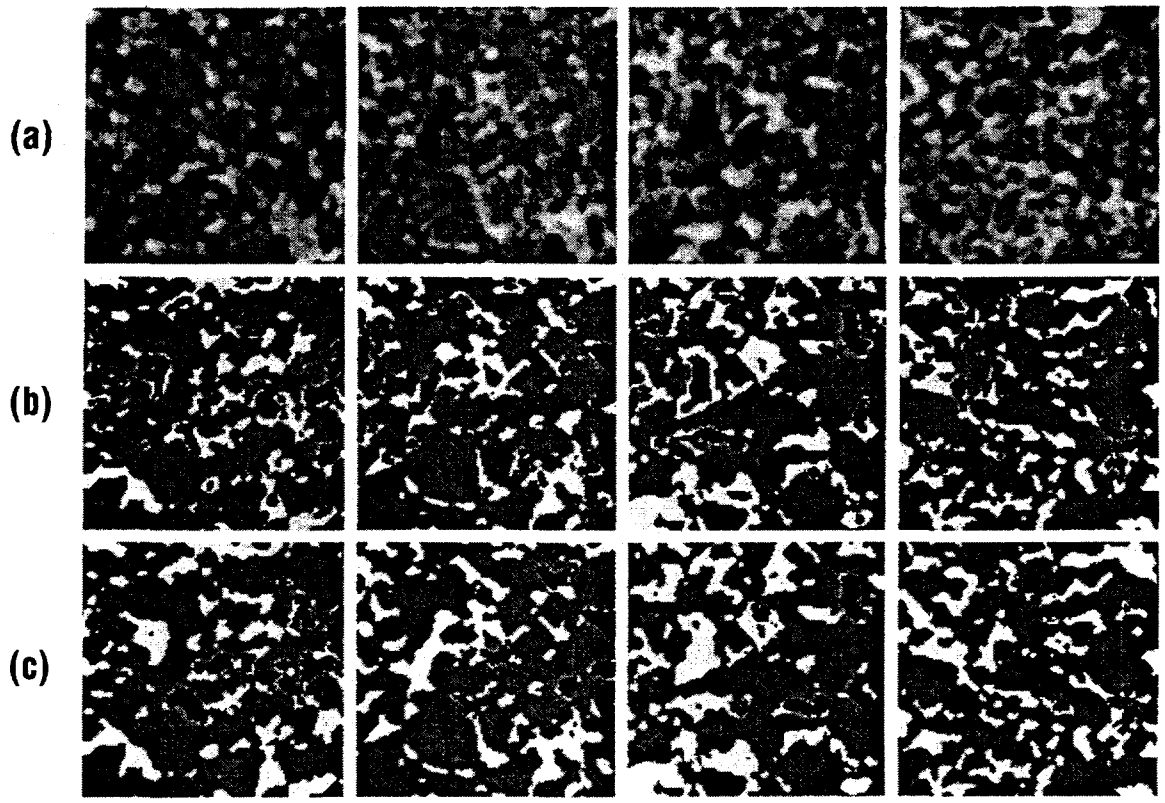

Figure 20

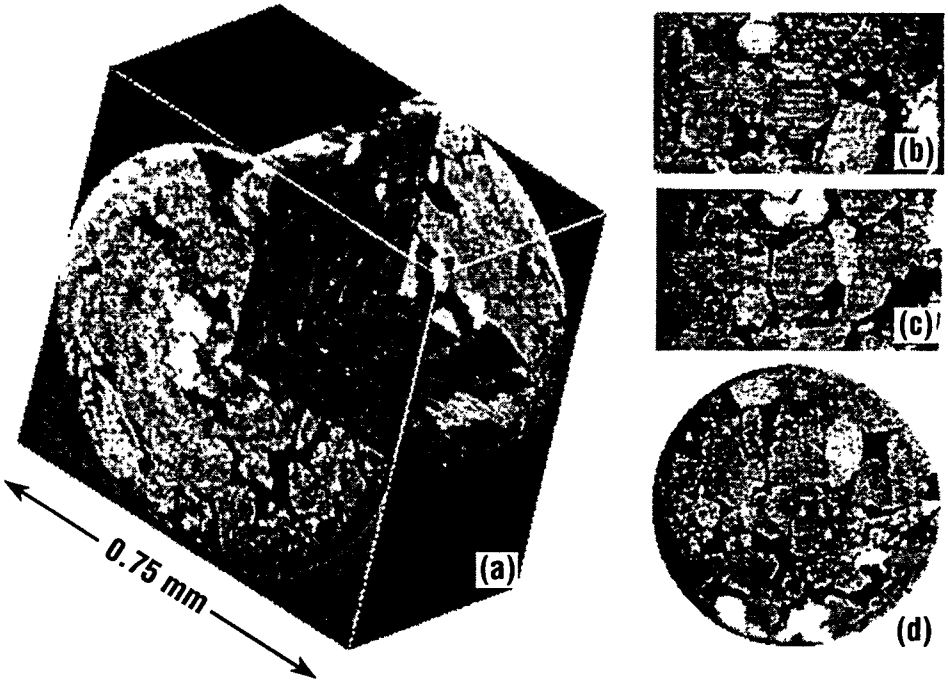

Figure 21

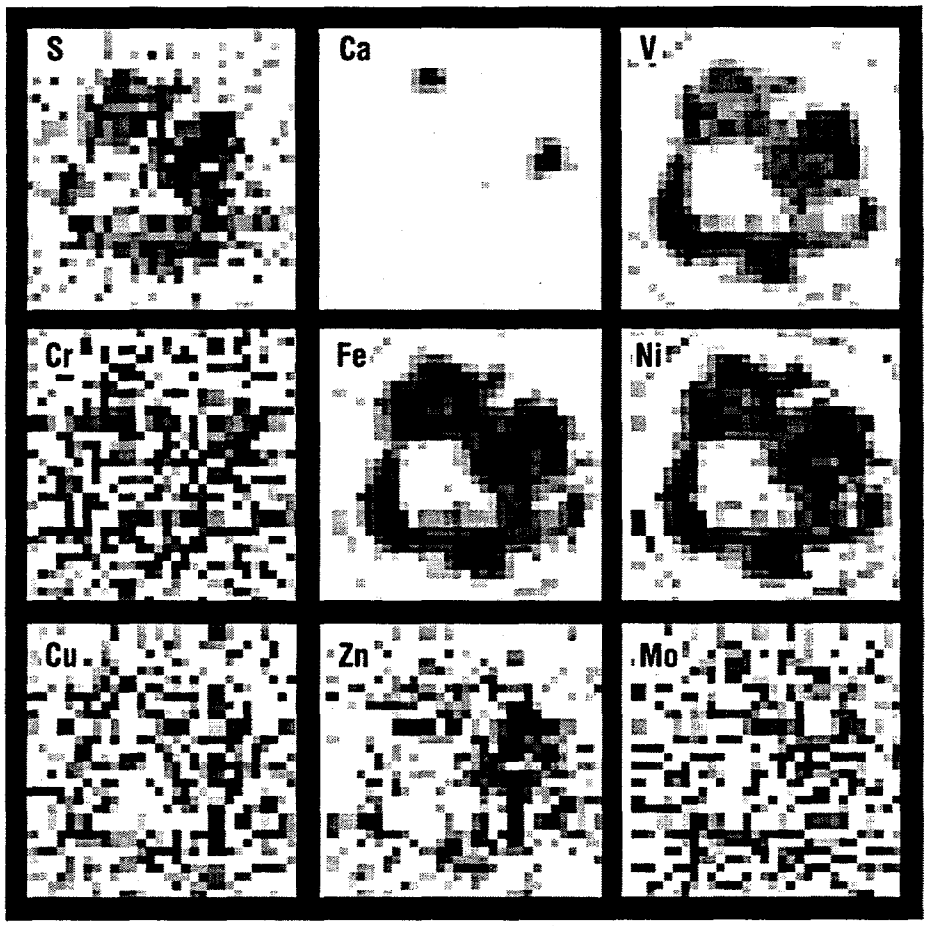

Figure 22

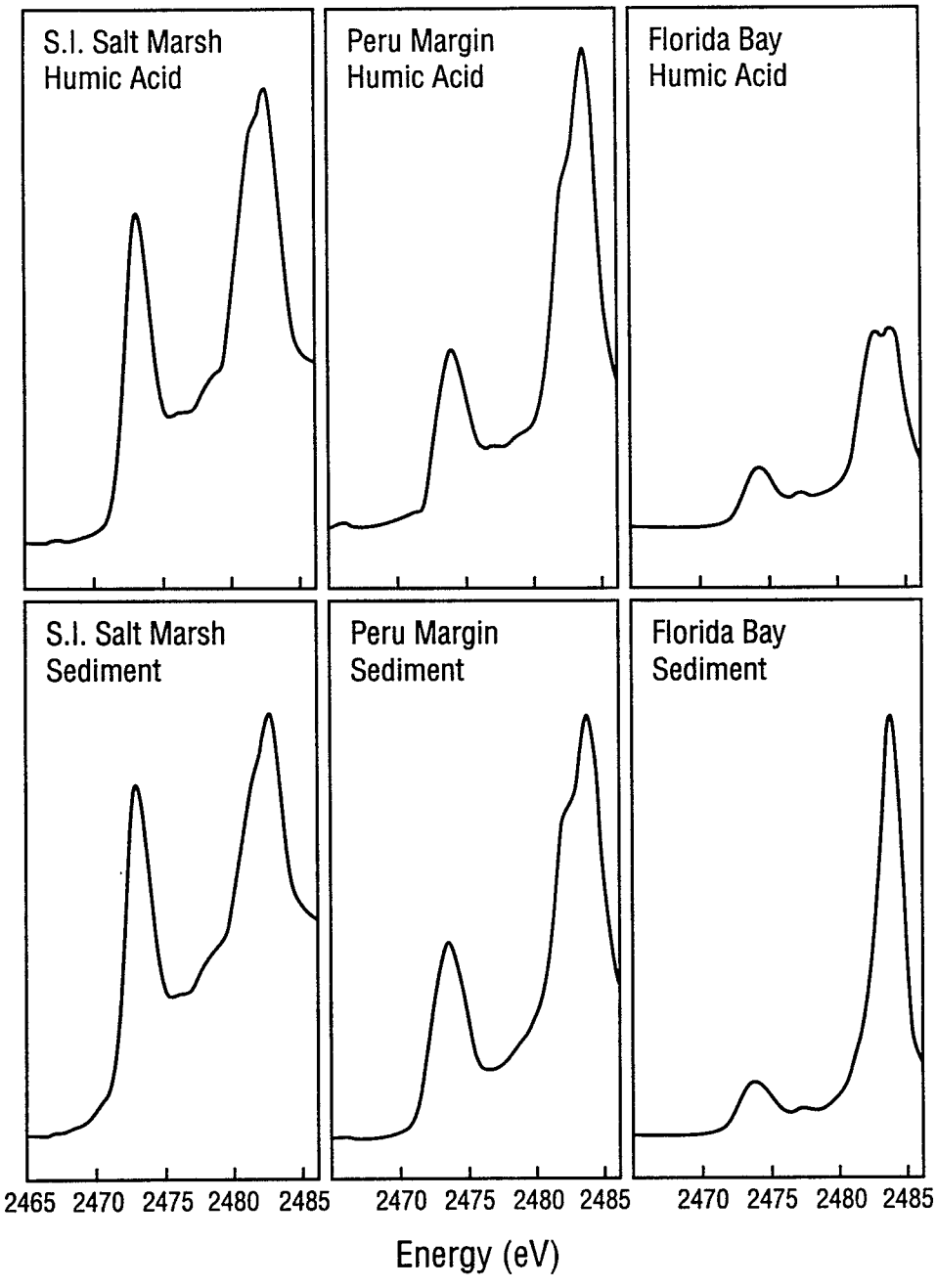
S.I. Salt Marsh
Humic Acid
Peru Margin
Humic Acid
Florida Bay
Humic Acid
S.I. Salt Marsh
Sediment
Peru Margin
Sediment
Florida Bay
Sediment
2465 2470 2475 2480 2485
2470 2475 2480 2485
2470 2475 2480 2485
Energy (eV)

Figure 23

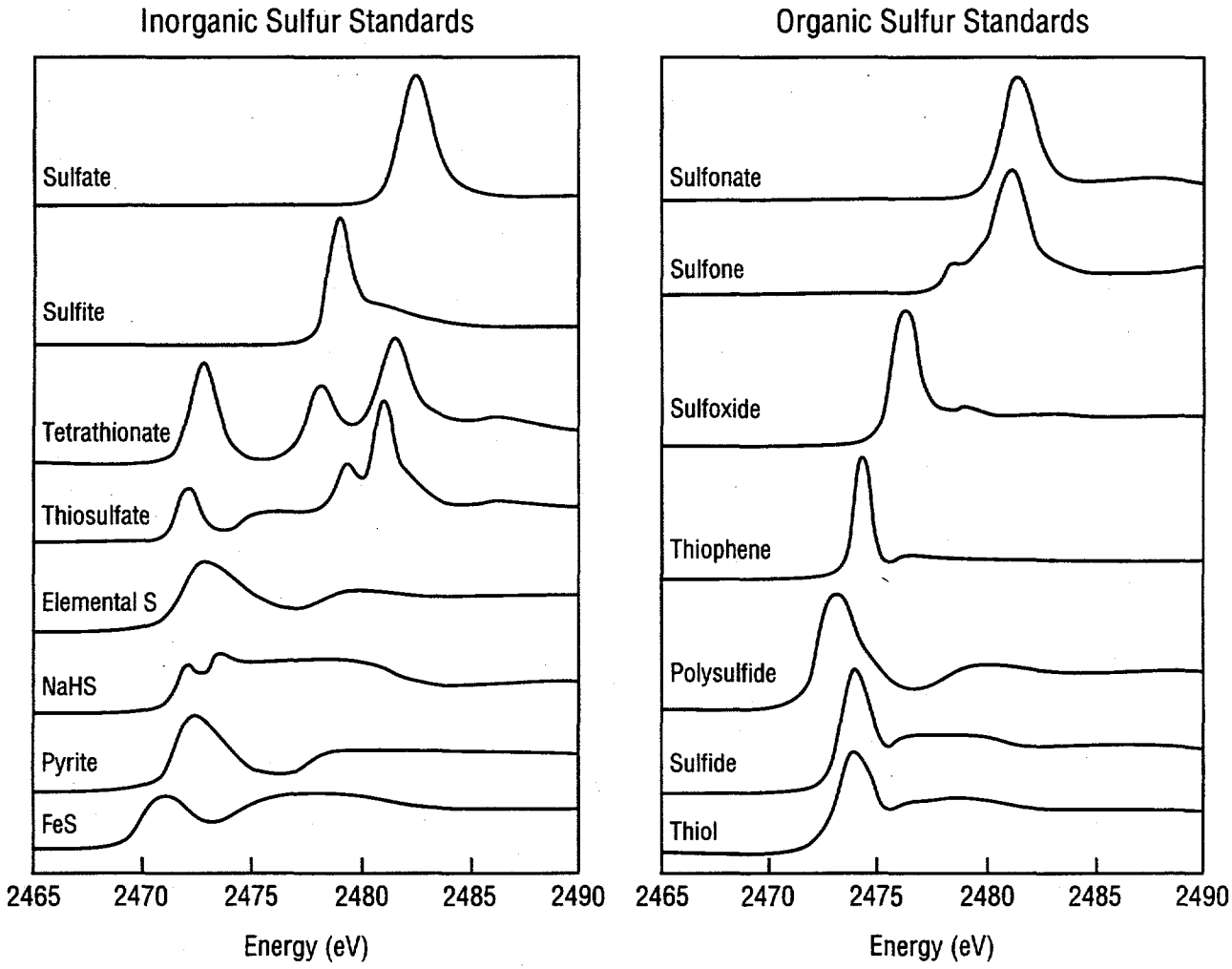
Inorganic Sulfur Standards
Sulfate
Sulfite
Tetrathionate
Thiosulfate
Elemental S
NaHS
Pyrite
FeS
2465
2470
2475
2480
2485
2490
Energy (eV)
Organic Sulfur Standards
Sulfonate
Sulfone
Sulfoxide
Thiophene
Polysulfide
Sulfide
Thiol
2465
2470
2475
2480
2485
2490
Energy (eV)

Figure 24

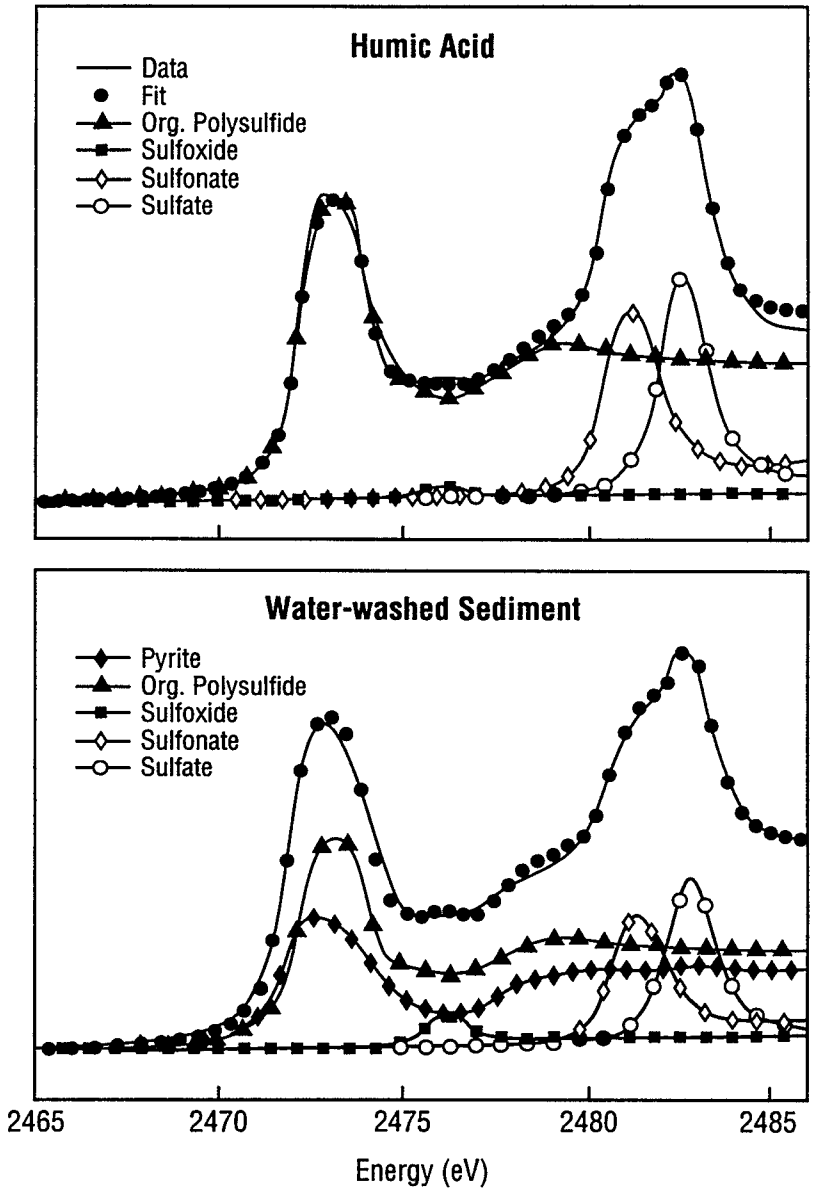
Humic Acid
Data
Fit
Org. Polysulfide
Sulfoxide
Sulfonate
Sulfate
Water-washed Sediment
Pyrite
Org. Polysulfide
Sulfoxide
Sulfonate
Sulfate
2465
2470
2475
2480
2485
Energy (eV)

Figure 25

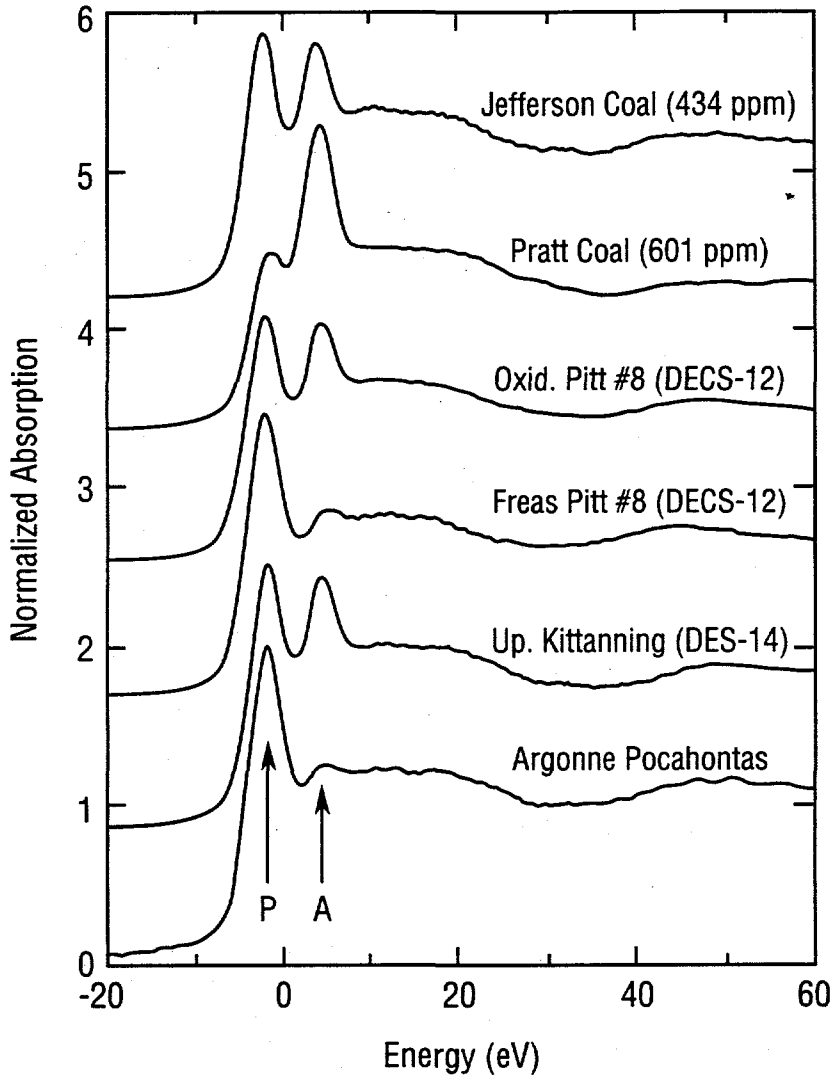
Jefferson Coal (434 ppm)
Pratt Coal (601 ppm)
Oxid. Pitt #8 (DECS-12)
Freas Pitt #8 (DECS-12)
Up. Kittanning (DES-14)
Argonne Pocahontas
P
A
Normalized Absorption
Energy (eV)
0
1
2
3
4
5
6
-20
0
20
40
60

Figure 26